CDF/PHYS/EXOTIC/CDFR/7027
June 9, 2004
Version 0.1

Search for Neutral MSSM Higgs Boson(s) in the $\tau\tau$ Decay Channel

Anton Anastassov, John Conway, Dongwook Jang, Amit Lath, Fedor Ratnikov, Zongru Wan

Department of Physics and Astronomy
Rutgers, The State University of New Jersey
Piscataway, NJ 08855 USA

Abstract

This note presents the current status of the search for MSSM Higgs bosons in the $\tau\tau$ decay channel.

1 Introduction

At hadron colliders the production of MSSM Higgs can be enhanced if the parameter $\tan\beta$ is large, due to the fact that the coupling of the Higgs to b quarks is proportional to $\tan\beta$. This can occur in gluon fusion to MSSM Higgs, which proceeds through a b loop as depicted in Figure 1.

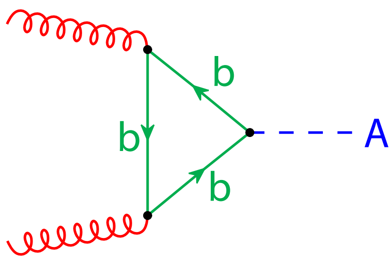

Figure 1: Gluon fusion production of pseudoscalar A.

Similar diagrams can lead to enhanced production of the light scalar h (if $m(A)$ is small) or heavy scalar H (if $m(A)$ is large). The complete phenomenology of these processes is reviewed in [1].

Another Higgs production mechanism that is enhanced with $\tan\beta$ is $b\bar{b} \to A$ - Figure 2.

The MSSM Higgs produced in this manner will decay predominantly to $b\bar{b}$ pairs, but will also have about an 8% branching ratio to $\tau^+\tau^-$. CDF has looked for this process in Run 1 [2] and set limits on the production rate as a function of Higgs mass.

We present in this note a search using CDF Run 2 data for enhanced production of MSSM Higgs, in the case where it decays to tau pairs. We select events with a hadronically decaying tau plus either an electron, a muon, or another tau. We distinguish such events from the large irreducible background

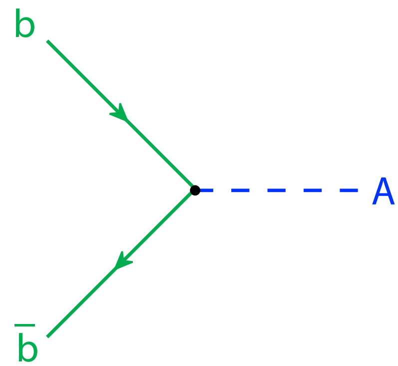

Figure 2: Lowest order diagram contributing to $b\bar{b} \to A$.

from $Z/\gamma^* \to \tau\tau$ by fitting the spectrum of the invariant "visible mass" formed from the tau, the lepton (or second tau), and missing transverse energy (treated as a four-vector).

2 Event topologies

In contrast to other leptons, taus have a rich decay spectrum. There are two groups of decays: leptonic ($\tau \to l\nu_\tau\nu_l(\gamma)$, $l = e, \mu$) and hadronic ($\tau \to X_h\nu_\tau$, X_h =system of hadrons). Throughout this note we use τ_e, τ_μ and τ_h as shorthand notations for taus detected in a particular decay channel.

The combinations of tau decay modes determine the detection channels for $\phi \to \tau\tau$ - Table 2.

The largest contribution comes from $\tau_h\tau_h$, however, detection in this mode is accompanied by higher QCD background. The modes $\tau_e\tau_h$ and $\tau_\mu\tau_h$ are the golden ones - they have significant contribution and contain an electron/muon that helps suppress QCD backgrounds. Despite its relatively small contribution, $\tau_e\tau_\mu$ is very interesting because it pro-

Mode	Fraction (%)	Comment
$\tau_e\tau_e$	3	useless
$\tau_\mu\tau_\mu$	3	useless
$\tau_e\tau_\mu$	6	low QCD bg
$\tau_e\tau_h$	23	golden
$\tau_\mu\tau_h$	23	golden
$\tau_h\tau_h$	41	challenging

Table 1: *Tau decay mode combinatorics and their importance for $\phi \to \tau\tau$ searches.*

Trigger	Efficiency	Note#
L1_CEM8_PT8	0.98 ± 0.01	6257
L2_CEM8_PT8_CES2	1.00 ± 0.02	6257
L3_ELECTRON8	0.99 ± 0.01	6324
L1_CMUP6_PT4	0.96 ± 0.01	6358
L3_CMUP8	0.997 ± 0.003	6621
L2_TRK5_DPHI10	0.98 ± 0.01	6510
L3_TRACK5_ISO	0.99 ± 0.01	6553
L1_CMX6_PT8	0.97 ± 0.01	6711

Table 2: *Trigger efficiencies.*

vides very efficient QCD suppression. All of the above modes will be explored in the final version of our analysis.

The modes $\tau_e\tau_e$ and $\tau_\mu\tau_\mu$ are not useful due to their small contributions and high ee and $\mu\mu$ DY backgrounds (in addition to $\tau\tau$ DY).

This Note includes the preliminary results on the "golden" modes.

3 Data and Monte Carlo

3.1 Data

There are several dedicated tau triggers for Run 2, allowing efficient selection of tau candidates for physics analyses. In this section we give brief overview of the triggers. The data used in the $\phi \to \tau_e\tau_h$ and $\phi \to \tau_\mu\tau_h$ channels is collected using the three *"lepton+track"* triggers. These triggers select a lepton candidate (electron, CMUP/CMX muon) and an isolated track. The "electron+track" trigger requires a XFT track with $P_T > 8$ GeV matched to a tower with $E_T^{EM} > 8$ GeV, forming the basis of the electron candidate. Level 2 reaffirms these selections and additionally requires CES cluster matched to the track. Level 2 also introduces the requirement for a second XFT track ("tau candidate side") with $P_T > 5$ GeV, separated by the "electron leg" by $\Delta\phi > 10$ deg. Level 3 adds charged track isolation on "tau side" (no tracks with $P_T > 1.5$ GeV in annulus $0.17 < R < 0.52$ rad) around the tau candidate, and imposes additional requirements on the "electron side".

There are two "muon+track" triggers implemented for the CMUP and CMX detector coverage. The track (tau) part is the same as for the "electron+track" trigger. At Level1 the triggers require hits in the CMU and CMP (CMX) chambers and associated stubs, matched to XFT track ($P_T > 6$ GeV). Level2 accepts all events. At Level3 the muon candidate must have $P_T > 8$ GeV.

The triggers were developed by the "Lepton plus Track" working group [3].

Marginal trigger efficiencies are listed in Table 3.1.

In this analysis we used Run 2 data up to run number 168889 and applied the EWG good run list. The data was originally processed with Production v4.8.4a. Subsequently we applied the TopRemake procedure using CDF Software v4.11.2.

3.2 Monte Carlo

Signal $\phi \rightarrow \tau\tau$ Monte Carlo was generated using Pythia 6.216 for the processes $qq, gg \rightarrow A$ (Pythia process numbers 156, 157), which are expected to have the largest contribution to the MSSM Higgs production cross section. We used fixed $\tan\beta$=30 and generated samples covering the mass region $115 < M_A < 200$ GeV. If the predicted cross-sections are not used, this choice mostly affects the mass width of the Higgs boson, and through it, the acceptance.

We used several MC samples to estimate backgrounds from EW and top processes Whenever needed, additional MC was produced with CDF Software v4.9.1hp3 and reprocessed with v4.11.2.

4 Particle identification

The particles of interest in this analysis are electrons (from τ_e), muons (from τ_μ), and the products of hadronically decaying taus. In this section we describe the particle identification requirements.

The selection criteria for electrons and muons closely follows the EWG recommendations. The Electron and Muon Groups have concentrated their efforts only on high-momentum leptons ($p_T > 20$ GeV). To maintain sufficient signal efficiency, we extend the reach to the lower-p_T region.

Having powerful electron/muon ID cuts is very helpful for controlling QCD backgrounds in our sample. We take full advantage of their discriminating power and apply additional (to the EWG recommendation) isolation cuts.

4.1 Electrons

The following is a list of the electron ID cuts used in the analysis. AC++ StdElectron was used as an initial electron candidate. Whenever possible, various quantities used in the selection are obtained using StdElectron methods.

Electron cuts

- $E_T > 10.0$ GeV
- $p_T > 8.0$ GeV
- $E_{had}/E_{EM} < 0.055 + 0.00045 * E$
- $L_{shr} < 0.2$
- $E_T^{iso} < 2.0$ GeV (cone 0.4)
- $0.5 < E/P < 1.5$
- $|\Delta X| < 2$ cm
- $|\Delta Z| < 3$ cm
- $\chi^2_{CESstrip} < 10$
- $|z_0| < 60$ cm
- $|d_0^{corr}| < 0.2$ cm
- ≥ 3 *stereo*, *axial* layers (> 6 hits)
- $p_T^{iso} < 1$ GeV (cone 0.4)
- $\sum p_T^{iso} < 2$ GeV (cone 0.4)
- fiducial in CES

- not a conversion

The additional isolation cuts require that there are no tracks with $p_T > 1$ GeV in isolation cone $R < 0.4$ around the direction of the electron (”veto” tracks). We also cut on the sum of the transverse momenta of all tracks in the isolation cone. Conversion removal is applied to electron candidates by forming all possible oppositely charged track pairs and rejecting the ones with $|S_{XY}| < 0.2\ cm,\ |\Delta\lambda| < 0.04$.

The data to MC scaling factor S_e for electron efficiency was determined using electrons from Z and Υ decays following the procedures outlined in [4]. We find the $S_e = 98.8 \pm 2.1\%$. Trigger efficiency is not included in this scaling factor. We assign 4% systematic uncertainty related to data/MC electron reconstruction and ID.

4.2 Muons

The analysis uses central muons reconstructed in the CMU+CMP and CMX detectors. Similar to the electron case, we apply track isolation cuts on top of the EWG baseline cuts.

Muon cuts

- $p_T > 10.0$ GeV
- $|z_0| < 60$ cm
- $|d_0^{corr}| < 0.2$ cm
- $E_{EM} < 2 + max(0, 0.0115 * (p - 100))$
- $E_{had} < 6 + max(0, 0.028 * (p - 100))$
- $E_{T,EM}^{iso} < 3.0$ GeV (cone 0.4)
- $E_{T,had}^{iso} < 3.0$ GeV (cone 0.4)
- $p_T^{iso} < 1$ GeV (cone 0.4)
- $\sum p_T^{iso} < 2$ GeV (cone 0.4)
- ≥ 3 *stereo*, *axaial* layers (> 6 hits)
- $|\Delta X_{CMU}| < 5\ cm$ and $|\Delta X_{CMP}| < 20$ cm (CMUP)
- $|\Delta X_{CMX}| < 6$ cm (CMX)

The data to MC scaling factors S_μ^{CMUP} and S_μ^{CMX} for the muon efficiencies were determined using muons from Z and Υ decays following the procedure in [5]. We find $S_\mu^{CMUP} = 91.0 \pm 2.7\%$ and $S_\mu^{CMX} = 101.8 \pm 3.9\%$. These factors do not include trigger efficiencies. We assign 4% systematic uncertainty for muon reconstruction and ID.

4.3 Taus

In a previous note [6] we described a set of baseline cuts for hadronic tau reconstruction. The selection criteria used in this analysis are similar, but not identical. The results are also affected by changes in π^0 reconstruction in the period between these notes.

”Tau reconstruction” refers to the reconstruction of the visible decay products X_h of taus experiencing semihadronic decays: $\tau \to X_h \nu_\tau$. X_h can be a $\pi^\pm/K^\pm$, or some short-lived intermediate resonance that decays directly (or through some intermediate states) to final states containing $\pi^{\pm,0}$, $K^{\pm,0}$. Table 4.3 lists the most important topological hadronic decay modes of tau leptons.

X_i	$\mathcal{B}_i$ (%)	$\mathcal{B}_i/\sum_j \mathcal{B}_j$ (%)
$h^-\pi^0$	25.86	40.4
h^-	11.75	18.3
$h^-h^+h^-$	10.01	15.6
$h^-2\pi^0$	9.39	14.7
$h^-h^+h^-\pi^0$	4.53	7.1

Table 3: *The top five most important topological final states of hadronic tau decays. $\mathcal{B}_i \equiv \mathcal{B}(\tau \to X_i\nu_\tau)$ are the tau branching fractions for the respective decay modes; h^- stands for π^- or K^-. Charge conjugate states are implied.*

Due to the Cabbibo and/or phase space suppression, the fraction of $K^\pm$ is small compared to $\pi^\pm$. In tau reconstruction we treat all charged tracks as pions.The π^0's in the final state decay predominantly to $\gamma\gamma$ ($\sim$ 98.8%). Most of the time, the opening angle between the photons is not sufficient for them to be resolved. In tau reconstruction we assume that the photons are always merged. This has small effect on the reconstructed mass (due to assigning π^0 mass to photons in some small number of cases). Dalitz decays of π^0's may lead to observation of additional tracks, but due to the small branching fraction ($\sim$ 1.2%) and low π^0 multiplicities in tau decays, we did not attempt to identify these decays.

Based on the major τ decay modes, taus are expected to produce characteristic track-multiplicity signature in the detector showing enhancements in the 1- and 3-track bins. Sometimes leakage into the 2- and 4-track bins occur due to track reconstruction inefficiencies, picking tracks from underlying event, etc.

Besides track multiplicity, the mass of the system can be used as another discriminating factor against QCD jets. The mass of the tau lepton is $m_\tau = 1.777$ GeV, and therefore, the decay products should have mass below this value.

Another implication of the small tau mass is that the decay products (for tau energies relevant for Z, W and Higgs studies at CDF) will form very narrow jets in the calorimeter.

Tau reconstruction and identification at CDF takes into account all these features.

The reconstruction starts with finding a seed calorimeter tower with transverse energy $E_T^{seed\ twr} > 6$ GeV. Adjacent shoulder towers with energies $E_T^{sh\ twr} > 1$ GeV are added to form a calorimeter cluster. Due to the narrowness of tau jets, the total number of towers contributing to the cluster N^{twr} is required to be less or equal to six.

The next step is to find a seed track for the tau candidate. This track must point to the calorimeter cluster and have momentum $p_T^{seed\ tr}$ exceeding some threshold. If several such tracks are found, the one with the highest p_T is chosen. The direction of the seed track is then used as a *reference direction* for all following steps. Other COT tracks are associated with the tau based on their closeness to the selected seed track. These shoulder tracks must have sufficiently high momentum $p_T^{sh\ trk}$, small separation $\Delta z^{sh\ trk}$ from the z-intercept of the seed track, and be within 3-D angle θ_{iso} with respect to the reference direction. Tracks within angle θ_{sig} are considered tau decay products, while ones with $\theta_{sig} < \theta < \theta_{iso}$ are treated as isolation tracks and used to veto tau candidates. Thus, the angles θ_{sig} and θ_{iso} define a signal cone and

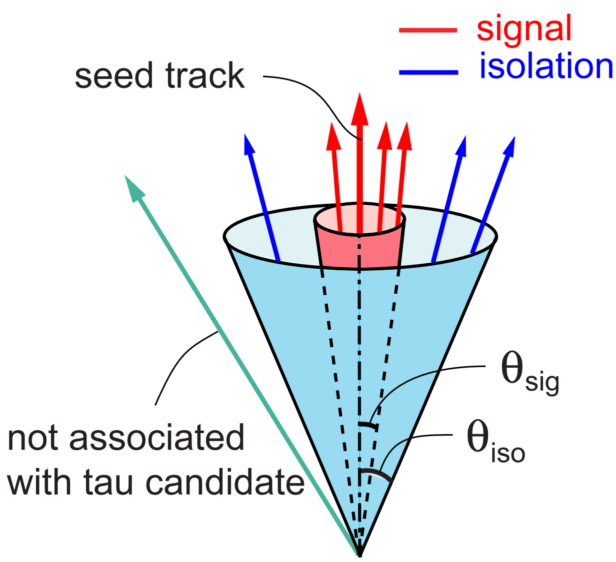

Figure 3: *Tau signal cone and isolation annulus for tracks and π^0's.*

isolation annulus as shown in Figure 3. The signal cone size depends on the cluster energy $E^{\tau\ cl}$.

Neutral pions are associated with the tau candidate following the same procedure as for shoulder tracks. They are reconstructed using CES clusters to determine their position, and CEM to assign energy. The π^0 reconstruction procedure is described in a separate note [8].

Tracks and π^0's in the signal cone are used to construct the four-momentum of the hadronic system. The four-momentum is used in subsequent event cuts and for the determination of the mass of the system $M(\text{trks} + \pi^0 s)$.

The following is a list of the tau reconstruction and ID cuts used in this analysis.

Tau cuts

- $\theta_{sig} = min(0.17, \dfrac{5.0 \text{ rad/GeV}}{E^{\tau\ cl}})$ rad [1]
- $\theta_{iso} = 0.52$ rad
- $p_T^{seed\ trk} > 6.0$ GeV [2]
- $p_T^{sh\ trk} > 1.0$ GeV
- $E_T^{\pi^0} > 1.0$ GeV
- $\Delta z^{sh\ trk} < 5.0$ cm
- $9.0 < |z_{CES}^{seed\ trk}| < 230.0$ cm
- $p_{T,trk}^{iso} < 1$ GeV
- $E_{T,\pi^0}^{iso} < 1$ GeV
- $\sum p_{T,trk}^{iso} < 2$ GeV
- $\sum E_{T,\pi^0}^{iso} < 2$ GeV
- $N_{sig}^{trk} = 1, 3$
- $|\sum Q^{trk}| = 1$
- $M(\text{trks} + \pi^0 s) < 1.8$ GeV
- $E_{iso}^{rel} = E_{iso}^{cone\ 0.4}/E^{\tau\ cl} < 0.1$
- $\xi > 0.2$

The variable ξ is designed to remove electrons [9] and is defined as

$$\xi = \frac{E_{had}}{\sum|\overrightarrow{p}|} = \frac{E_{tot}}{\sum|\overrightarrow{p}|}\left(1 - \frac{E_{EM}}{E_{tot}}\right), \qquad (1)$$

where E_{tot}, E_{EM}, E_{had} are the total, electromagnetic and hadronic tau cluster energies,

[1] In addition, we require $0.05 < \theta_{sig} < 0.17$ rad for tracks and $0.1 < \theta_{sig} < 0.17$ rad for π^0's

[2] Seed track quality: ≥ 3 stereo, ≥ 3 axial layers with more than 6 hits

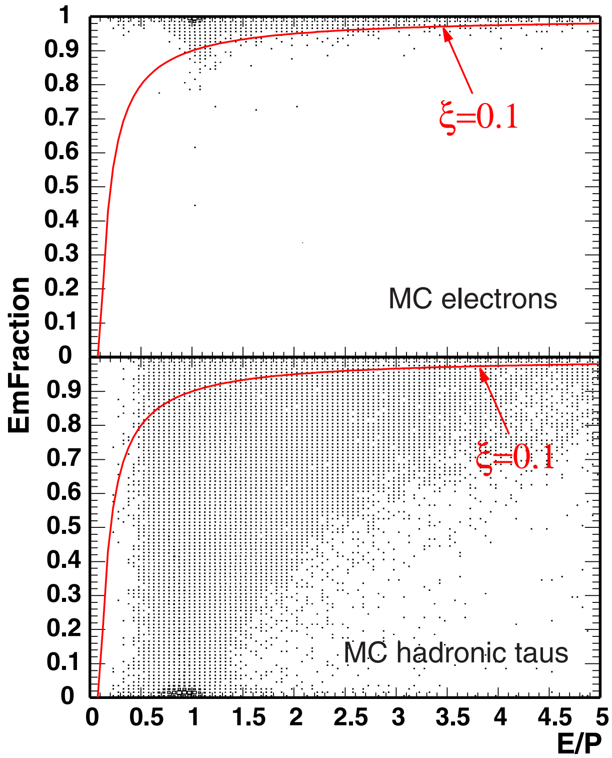

Figure 4: *Electromagnetic fraction vs. E/P for MC taus and electrons. after all selection cuts are applied except the ξ cut. Entries with $\xi > 0.1$ are in the region below the solid lines.*

and $\overrightarrow{p}$ are the momenta of charged tracks associated with the tau. Figure 4 demonstrates the discriminating power of the ξ cut.

To further suppress electrons accompanied by bremsstrahlung, we reject $\pi\pi^0$ tau candidates when the π^0 is within $|\Delta z_{CES}| < 2.0$ cm of the projection of the track **and** in ϕ lies between the CES intersect of the track helix and its tangential. [3]

[3]Due to CES position resolution, the veto region is extended by 0.01 rad beyond the point of the tangential intersect at CES.

5 Event cuts

Apart from the irreducible background from $Z/\gamma^* \to \tau\tau$ the other **major** backgrounds in this analysis are $Z/\gamma^* \to ee$, $Z/\gamma^* \to \mu\mu$, $W \to e\nu + jet(s)$, and "QCD" ($p\bar{p} \to njets$). The event cuts are designed as a compromise between effective suppression of **these** backgrounds and maintaining sufficient signal efficiency. Other backgrounds, such as $t\bar{t}$, WW, WZ, and ZZ are taken into account in the analysis (and are also suppresses by some of the cuts), but due to their small contribution played limited role in designing the cuts.

5.1 Anti $Z \to ll$ cuts ($l = e, \mu$)

These cuts are directed at suppressing $Z \to ll$ events where an electron or a muon was misidentified as a tau.

The procedure is similar for the electron and muon case. In the muon case, we form the invariant mass M_{test} of identified muons with reconstructed 1-prong taus, using track momenta. Events in the mass region $|M_{test} - M_Z| < 25$ GeV are vetoed. When electrons are involved, all tau candidates, regardless of track multiplicity are used to form M_{test} (this is prompted by possible presence of "triads"). The tracks are used to determine the direction of the electron candidates, and the magnitude is assigned from the EM energy in the calorimeter.

5.2 QCD suppression cuts

Jets are suppressed to a significant degree by the tau ID cuts. However, at low E_T their number is so large that event cuts are needed to clean up the sample. We define

$$\tilde{H}_T = |P_T^{vis}(\tau_1)| + |P_T^{vis}(\tau_2)| + MET.$$

This sum is **not** H_T of the event: it only includes quantities related to the expected decay products of ϕ (or Z). We intentionally avoided inclusion of jets accompanying the ϕ/Z to avoid issues with MC modeling. However, at a later time including more complete information may prove beneficial. Figure 5 shows the expected distributions for Z, ϕ, and a QCD.

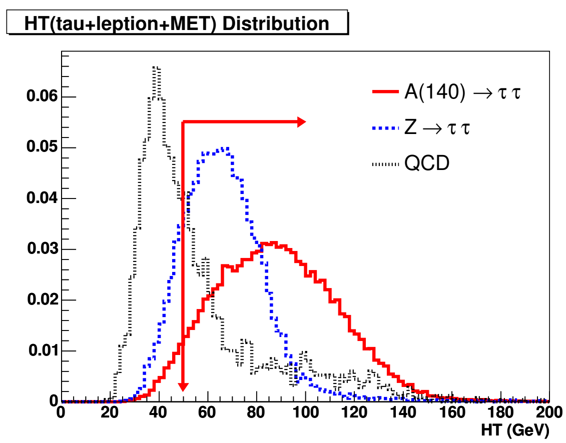

Figure 5: *Effect of the H_T cut on Z, $\phi(140)$, and QCD-dominated data sample. All distributions are normalized to unit area.*

The QCD distributions are obtained from the data sample, but without applying tau ID cuts to the jets. While it contains some real taus, it is largely dominated by jets, especially at the low-$\tilde{H}_T$ side, which we would like to reject. The suggested cut $\tilde{H}_T >$ 50 GeV leads to small loss of signal efficiency, while providing considerable QCD suppression. The impact of this cut on signal is further reduced when probing for higher-mass ϕ.

5.3 ζ cut

The "ζ cut" in an attempt to discriminate events with MET that are not consistent with a particle decaying to two taus. It is mostly targeted at $W \to l\nu + jet(s)$, but also helps to suppress QCD, $t\bar{t}$ and di-boson events.

We define a bisection axis $\vec{\zeta}$ in the transverse plane for the directions of the visible tau decay products.

The transverse momentum of ϕ (or any other particle decaying to two taus) is

$$\vec{P}_T^{\phi} = \vec{P}_T^{vis}(\tau_1) + \vec{P}_T^{vis}(\tau_2) + \vec{\not{E}}_T,$$

where we assume that $\vec{\not{E}}_T$ is the sum of the transverse momenta of the neutrinos from tau decays. The transverse momentum of the tau visible products is

$$\vec{P}_T^{vis\ \tau} = \vec{P}_T^{vis}(\tau_1) + \vec{P}_T^{vis}(\tau_2).$$

The projections of $\vec{P}_T^{\phi}$ and $\vec{P}_T^{vis\ \tau}$ onto the defined $\vec{\zeta}$ axis are

$$P_{\zeta}^{\phi} = \vec{P}_T^{\phi}.\vec{\zeta}$$

and

$$P_{\zeta}^{vis\ \tau} = \vec{P}_T^{vis\ \tau}.\vec{\zeta},$$

respectively.

Figure 6 provides illustration of these definitions.

Figure 7 shows the P_{ζ} *vs* $P_{\zeta}^{vis\ \tau}$ distribution for $\phi \to \tau\tau$, and $W \to l\nu + jet(s)$ MC events. The distributions are plotted after applying the other event cuts. The graphical cut shown on these plots results in small efficiency loss and substantial background suppression.

The rational behind this cut is simple: both the neutrinos and the visible decay

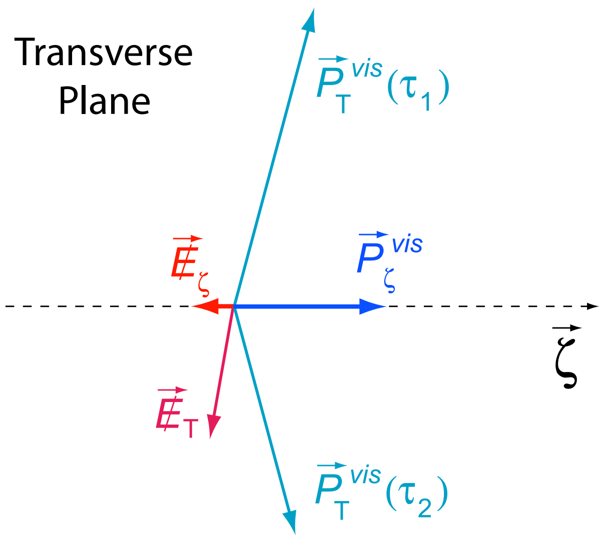

Figure 6: *Illustration of the definition of parameters used in the* ζ *cut.*

products from tau decays go at small angles from the initial tau direction (at our energy scale). Therefore, the sum of the neutrino's momenta should not go opposite to the direction of the sum of visible products. The defined acceptance region implicitly takes into account factors like direction and energy resolution of reconstructed taus, MET resolution, etc. The cut placement is determined by inspecting the predicted distributions and minimizing the signal losses. Figure 7 shows the effect of the cut on signal (Higgs) and $W + jet(s)$ background.

5.4 Charge Requirements

The lepton and the hadronic decay products of the tau pair are required to have opposite charge: $Q_l Q_{\tau_h} = -1$. This cut is mostly directed at $jet \to \tau$ fakes.

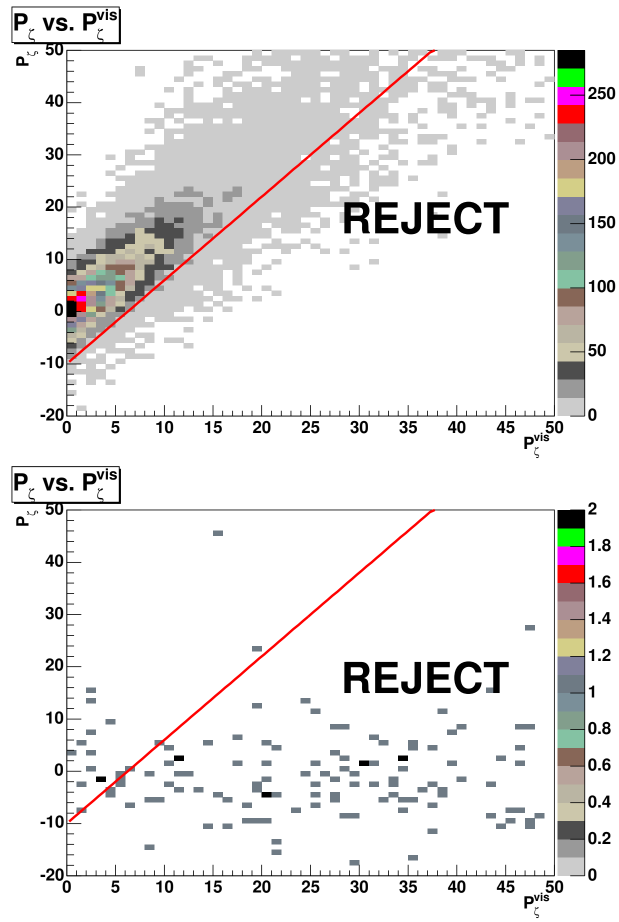

Figure 7: *Effect of the* ζ *cut on signal* $\phi(140)$ *(top) and* $W + jet(s)$ *MC events (bottom).*

6 Tau Reconstruction Efficiency and Fake rate

.

We define efficiency and fake rate as *absolute* and *relative*. Absolute efficiency (fake rate) are defined with respect to taus (jets) passing fiduciality requirements. These are measures of the performance of tau reconstruction, and are reflected in overall signal acceptance and background contamination.

Relative efficiency and fake rate are defined with respect to objects that have some restrictions already imposed:

- There is a "TauObject" matched to the tau or jet
- Pass the ξ (anti-electron) cut
- Pass the "track" part of the "lepton+track" trigger requirements
- $|z_0^{seed\ trk}| < 60.0$ cm
- $9.0 < |z_{CES}^{seed\ trk}| < 230.0$ cm
- Seed track quality: ≥ 3 stereo, ≥ 3 axial layers (> 6 hits)

We refer to objects passing these cuts as "loose taus", as opposed to "tight taus" that pass the full tau ID cuts described in Section 4

The first requirement is important because it allows us to use the same parameters when defining efficiency and fake rate. Typically, about $\sim 50\%$ of generic jets are reconstructed as "TauObjects". The second requirement excludes small parameter space that is not relevant for fake estimation in our final sample and reduces electron contamination. The third requirement ensures that we can use the same data sample for extracting the signal and determining $jet \rightarrow \tau$ fakes [4]. The rest of the requirements ensure geometrical and tracking quality consistency with the final sample.

[4] We are planning to use data coming on another trigger to cross check the QCD estimates and drop this requirement

6.1 Tau Reconstruction Efficiency

Tau reconstruction efficiency is determined from MC simulation and cross checked using taus from $W \rightarrow \tau\nu$ decays in the data.

Absolute efficiency is estimated for taus that originate from the luminous region ($|Z_0| < 60.0cm$) and pass the fiduciality requirements (highest P_T track projection to the CES detector $9.0 < |z_{CES}^{trk}| < 230.0$ cm). Absolute efficiency can be defined as a function of reconstructed or generated energy and is a true measure of reconstruction performance. It is implicitly included when event selection efficiency is estimated from the MC simulation. Differences between data and MC efficiency are accounted for by a scaling factor of 0.95 ± 0.10, determined from $W \rightarrow \tau\nu$ decays (see Appendix C).

Relative efficiency is determined with respect to loose taus, and is therefore, numerically higher than absolute efficiency. It enters in the calculation of QCD backgrounds. It is parameterized in terms of *measured* quantities: E_T^{cl}, η_{det} (we are experimenting with adding more parameters). The efficiency is determined from the ratio of number of tight to number of loose taus in bins (partitions) in the 2D parameter space. This parametrization of the efficiency and the corresponding distributions (Figure 8 are useful only in the procedure for estimating the $jet \rightarrow \tau$ fakes.

6.2 $jet \rightarrow \tau$ Fake rate

The $jet \rightarrow \tau$ fake rates are studied using the JET20, 50, 70, 100 samples. To reduce trigger bias, only non-trigger jets are used. A "trigger jet" is the one responsible for the se-

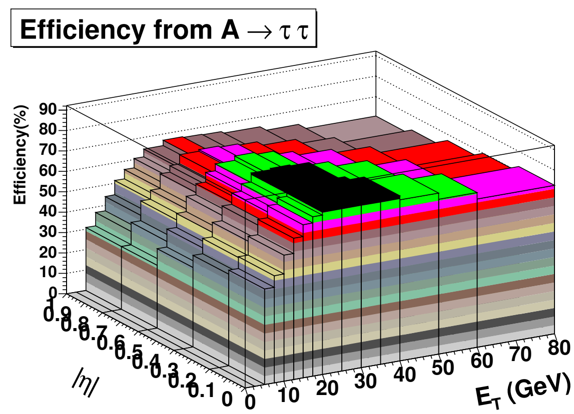

Figure 8: *Relative efficiency as a function of tau cluster E_T and detector η.*

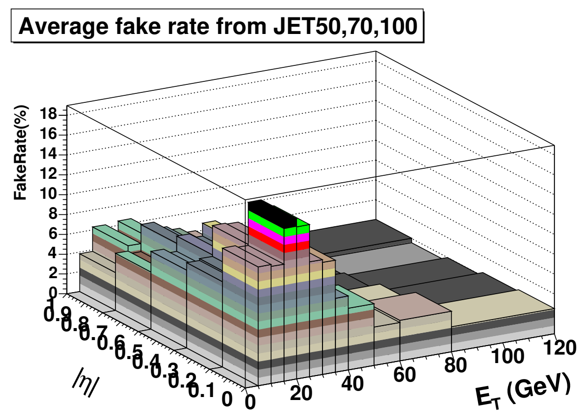

Figure 9: *Relative fake rate as a function of "tau" cluster E_T and detector η.*

lection of the event: it is the only jet in the event fulfilling all L1, L2, L3 requirements. If there is more than one jet in the event passing L1, L2, L3, all jets are considered "non-trigger" and used in the fake rate studies. This procedure does not seem to eliminate trigger bias completely. In particular, we have observed that predictions based on fake rates obtained using JET20 alone significantly overestimate backgrounds in control regions. As a result, we do not use JET20 in our fake estimates.

Similar to the efficiency, fake rates are parameterized in terms of E_T^{cl}, η_{det} - Figure 9.

The difference between predicted and observed events in control samples are used as estimates of the systematic uncertainty. Details on fake rate consistency checks are presented in Appendix A.

7 Background estimation methods

7.1 $Z \rightarrow \tau\tau$

This group includes $Z \rightarrow \tau\tau$ decays to the same final states as the signal. Apart from di-tau mass (and related parameters) these events are practically indistinguishable from the signal [5]. This is the largest expected background for this analysis. We do not make any attempt to suppress the Z backgrounds. Any differences in di-tau mass related parameters are used at the time of signal extraction/ limit setting procedure. The contribution of these backgrounds is estimated using the MC simulation along with experimental results on the Z production cross sections from $Z \rightarrow ll$ (lepton universality is assumed).

[5] In principle, there are some differences due to boson spin resulting in differences in $\tau\tau$ polarization. However, high statistics (and energy resolution) are needed to take advantage of these effects.

7.2 $Z \to ee$, $Z \to \mu\mu$

An electron or a muon can be reconstructed as a hadronic tau. We use MC samples to estimate events that survive $Z \to ll$ removal event cuts.

7.3 Di-boson and $t\bar{t}$

These are small backgrounds (due to small production cross sections). There are two mechanisms for these events to enter our sample: when the final state contains the particles expected in our signal final state, e.g. $e\tau_h$, $\mu\tau_h$, etc., or if a e or μ "fakes" a hadronic tau. These backgrounds are substantially suppressed by the "ζ cut". It is important to have them under control, because they could potentially be reconstructed as high-mass ditau pairs. These backgrounds are estimated using MC samples. When available, experimental production cross sections are used.

7.4 Backgrounds with $jet \to \tau$ fakes

There are three quite different processes that contribute to this group:

- $W \to l\nu + jet(s)$: one of the jets fakes a hadronic tau
- γ + jet: the photon undergoes conversion with one soft/undetected leg, resulting in reconstruction of an isolated electron; the jet fakes a hadronic tau
- $p\bar{p} \to n$ jets: one jet fakes a tau, another one fakes an e/μ

There are two approaches that can be taken to estimate these backgrounds. The first one is to try to estimate the contributions from each source separately. The other one is to apply jet $\to \tau$ fake rates to samples of events that pass event cuts but have jets on the "tau side". We chose to use the second ("fake rate method") in this analysis.

We use the signal sample to estimate the $jet \to \tau$ backgrounds. The relative fake rates are applied to loose tau candidates to predict the number (and distributions) of fake taus in the final sample.

Due to the relatively tight track isolation at trigger level and the power of our event selection cuts, the loose tau sample contains large fraction of real taus. We account for this contamination through the procedure described below.

Let us start with a simplified case, and consider an initial sample passing loose tau cuts, and a final sample produced after applying the tight cuts. The number of real taus and $jet \to \tau$ fakes that survive this transition depend on the efficiency and fake rate.

Let $\hat{N}$ be the number of tau candidates passing the loose tau cuts, and denote the number of candidates passing the tight tau cuts by N. There are three sources that contribute to the observed events: real taus, leptons ($l = e, \mu$), and "jets". This is reflected in the following set of equations

$$\hat{N} = \hat{N}^{\tau} + \hat{N}^{jet} + \hat{N}^{l}$$

$$N = N^{\tau} + N^{jet} + N^{l}$$

$$N^{\tau} = \epsilon \hat{N}^{\tau}$$

$$N^{jet} = f \hat{N}^{jet},$$

where the last two expressions are the definitions of relative efficiency and fake rate.

Then it is easy to show that the jet background can be written as

$$N^{jet} = \frac{f}{\epsilon - f}[\epsilon \hat{N} - N] - C_l,$$

where C_l is a correction for e, μ contributions (which is small for the considered processes). It has the form

$$C_l = \frac{f}{\epsilon - f}[\epsilon \hat{N}^l - N^l],$$

where the leptons passing as loose and tight taus can be obtained from MC simulation.

If we take into account that efficiency and fake rate are actually functions of the parametrization variables (whatever they might be) and write the equations for infinitesimally small regions in parameter space, we get the same expressions for the fake tau density in terms of the event densities $\hat{n}$ and n (instead of number of events)

$$n^{jet}(\Omega) = \frac{f(\Omega)}{\epsilon(\Omega) - f(\Omega)}[\epsilon(\Omega)\hat{n}(\Omega) - n(\Omega)] - c_l,$$

where Ω denotes a point in the efficiency/fake rate parametrization space. The densities $\hat{n}(\Omega)$ and $n(\Omega)$ are given by

$$\hat{n}(\Omega) = \sum_i^{\hat{N}} \delta(\Omega - \Omega_i)$$

$$n(\Omega) = \sum_i^{N} \delta(\Omega - \Omega_i).$$

To obtain the number of $jet \to \tau$ fakes in the final sample we substitute the above densities in the expression for $n^{jet}(\Omega)$ and integrate over the parameter space. The QCD estimation reduces to sum over all loose taus which enter with weight

$$w_i^{\overline{ID}} = \frac{f(\Omega_i)\epsilon(\Omega_i)}{\epsilon(\Omega_i) - f(\Omega_i)}$$

if the candidate did not pass tight tau ID cuts, and

$$w_i^{ID} = \frac{f(\Omega_i)(\epsilon(\Omega_i) - 1)}{\epsilon(\Omega_i) - f(\Omega_i)}$$

if it did. It is straight forward to apply the "lepton correction".

Using these weights we can obtain the distributions for various event variables.

8 Observed $\tau_e\tau_h$ and $\tau_\mu\tau_h$ Candidate Events

The track multiplicity distributions for tau candidates in the selected events are presented in Figure 11. These are the only plots where track multiplicity ($N_{trk} = 1, 3$) and opposite charge ($Q_{\tau_l}Q_{\tau_h} = -1$) requirements are not applied. They are presented to demonstrate that the final samples are dominated by events with hadronically decaying taus. Subsequent plots show distributions for events with track multiplicity and opposite charge requirement applied. The plots show data along with expected backgrounds as indicated on the plots. The electron and muon channels are plotted separately, and we also include plots for the individual contributions for events with CMUP and CMX muons. This presentation scheme is used in all plots. The MC samples are normalized to the respective measured cross-sections. Trigger efficiency and data/MC scaling factors accounting for differences between data and MC particle reconstruction and ID are included. The trigger efficiencies have been measured only for 72 pb^{-1}. In Appendix D we explain the steps that were taken to extrapolate the efficiencies to cover the entire data sample. The $jet \rightarrow \tau$ fakes are determined using the described procedure with no additional scaling or adjustment to the predictions.

The predicted backgrounds and observed events in data are summarized in Table 4.

sources	$\tau_h\tau_e$	$\tau_h\tau_\mu^{CMUP}$	$\tau_h\tau_\mu^{CMX}$	all muons	all
$Z \to \tau\tau$	132.3 ± 1.7	74.3 ± 1.2	29.9 ± 0.8	104.1 ± 1.5	236.4 ± 2.3
$Z \to ll$	1.8 ± 0.2	3.4 ± 0.3	1.4 ± 0.2	4.9 ± 0.3	6.7 ± 0.4
$t\bar{t}, VV$	0.7 ± 0.1	0.6 ± 0.1	0.1 ± 0.0	0.8 ± 0.1	1.5 ± 0.1
$jet \to \tau$	12.0 ± 1.9	5.5 ± 1.3	1.5 ± 0.9	7.0 ± 1.6	18.9 ± 2.5
Sum BG	146.8 ± 2.6	83.8 ± 1.8	33.0 ± 1.2	116.8 ± 2.2	263.5 ± 3.4
DATA	133	64	39	103	236

Table 4: *Predicted backgrounds and observed events after applying all selection cuts. The errors are statistical only.*

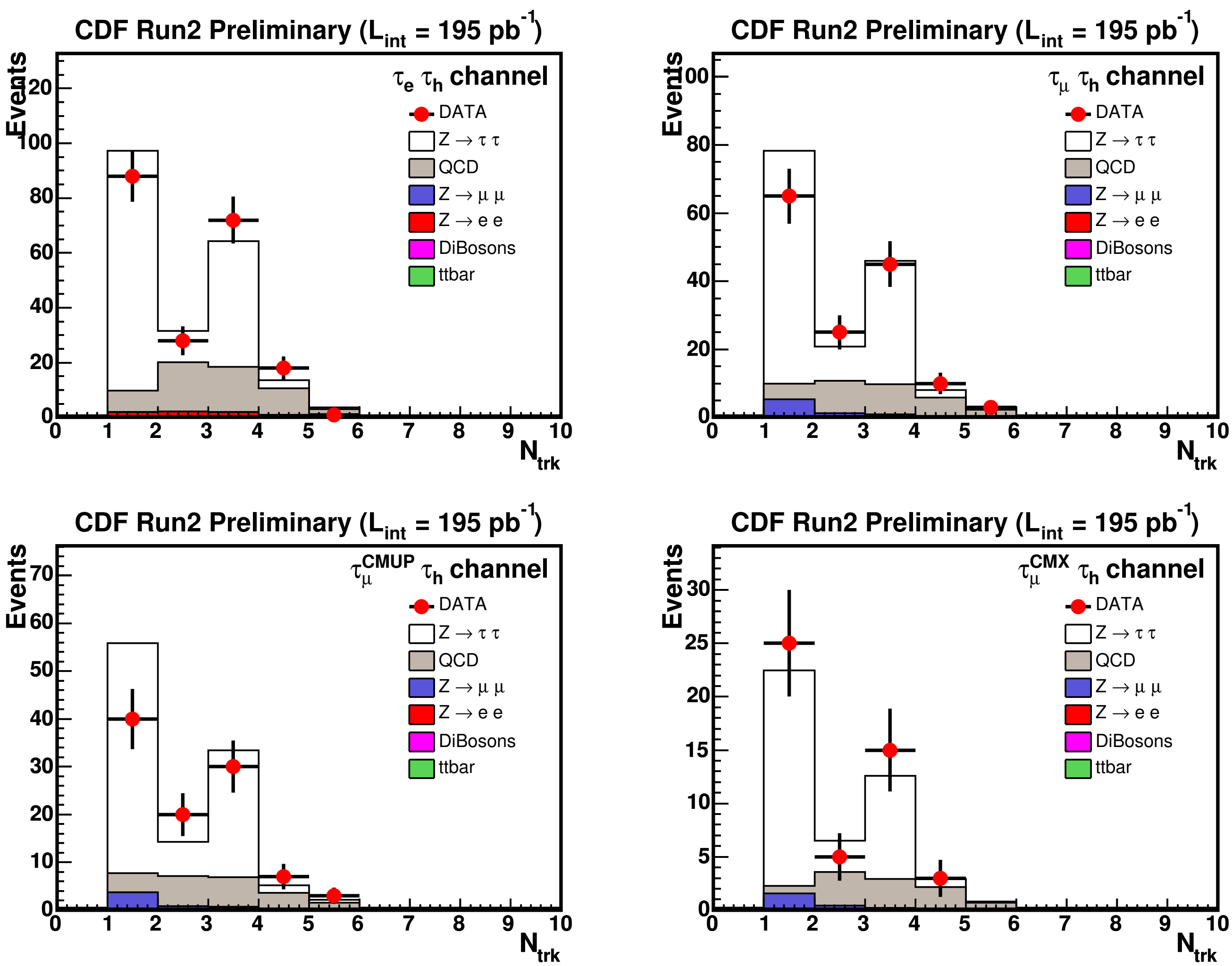

Figure 10: *Track multiplicity for tau candidates.*

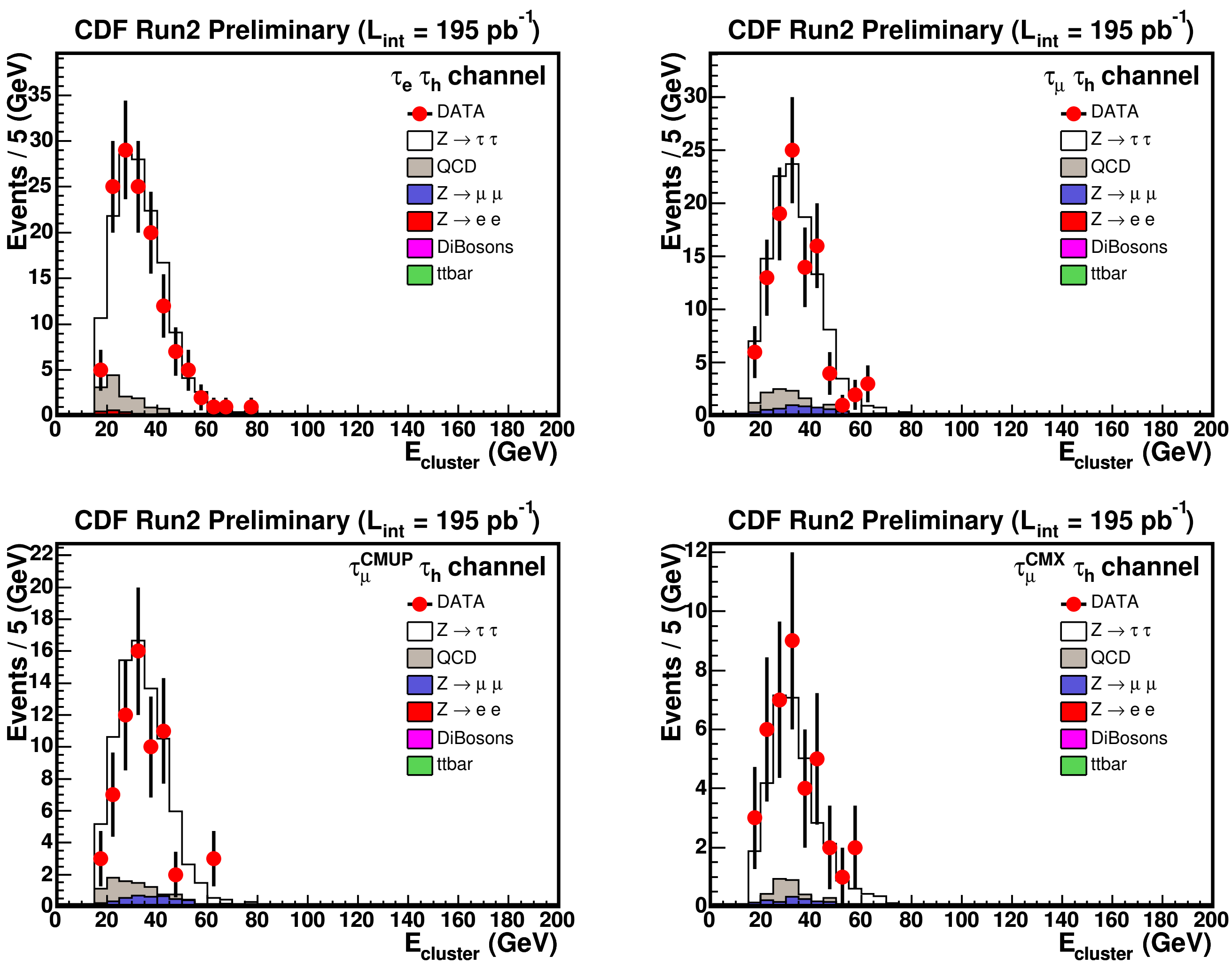

Figure 11: *Tau cluster energy.*

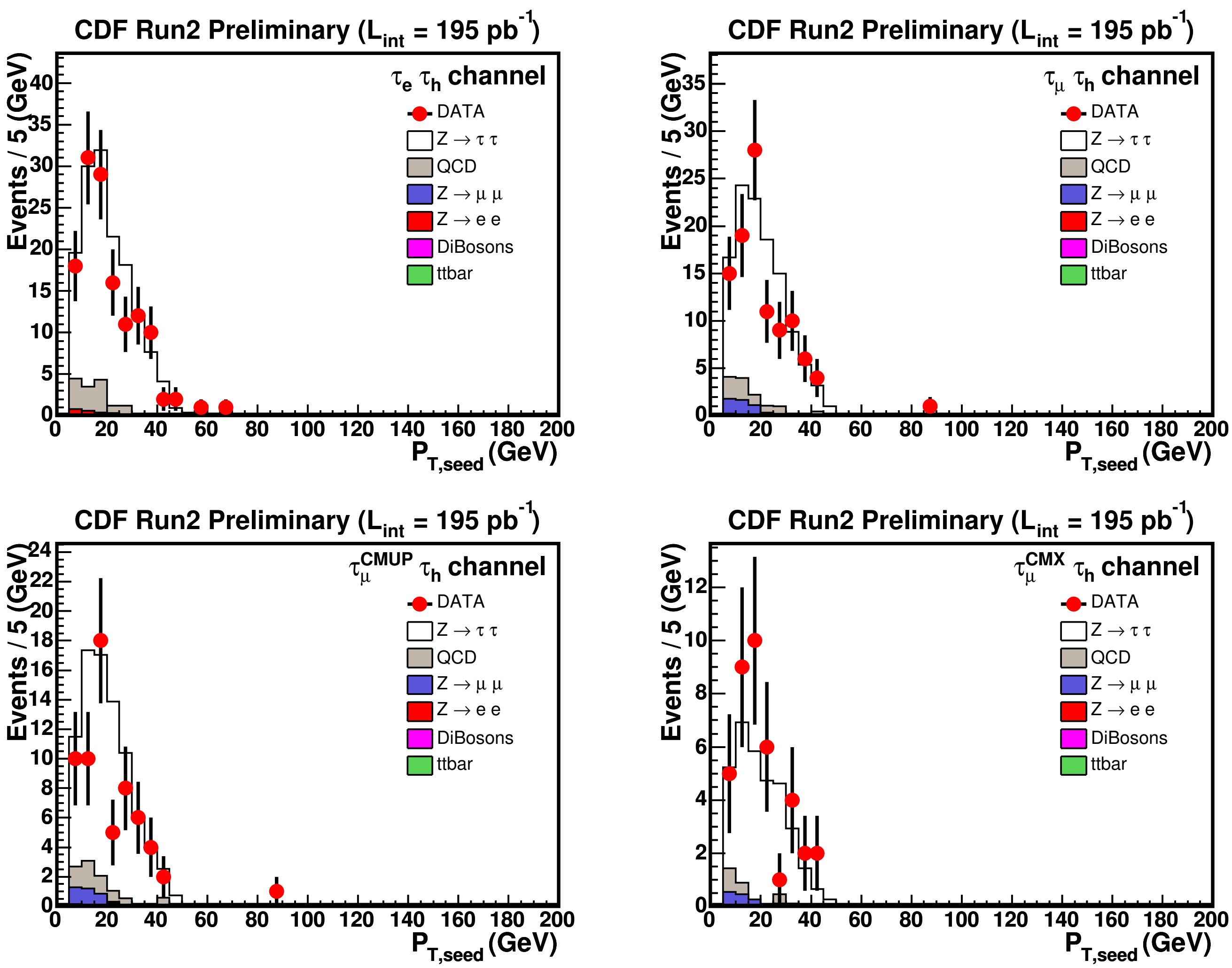

Figure 12: *Transverse momentum of tau seed track.*

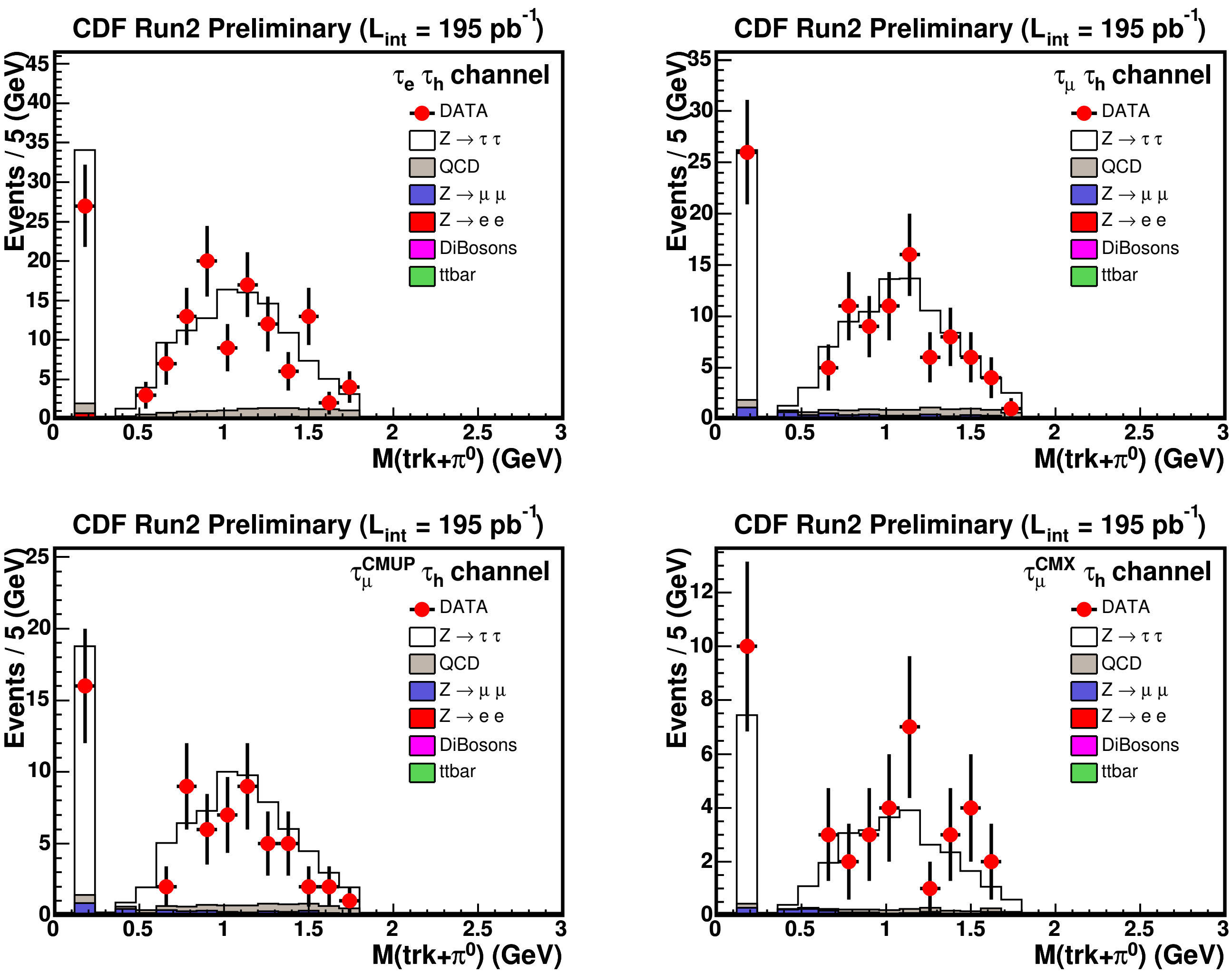

Figure 13: *Mass of tau candidates.*

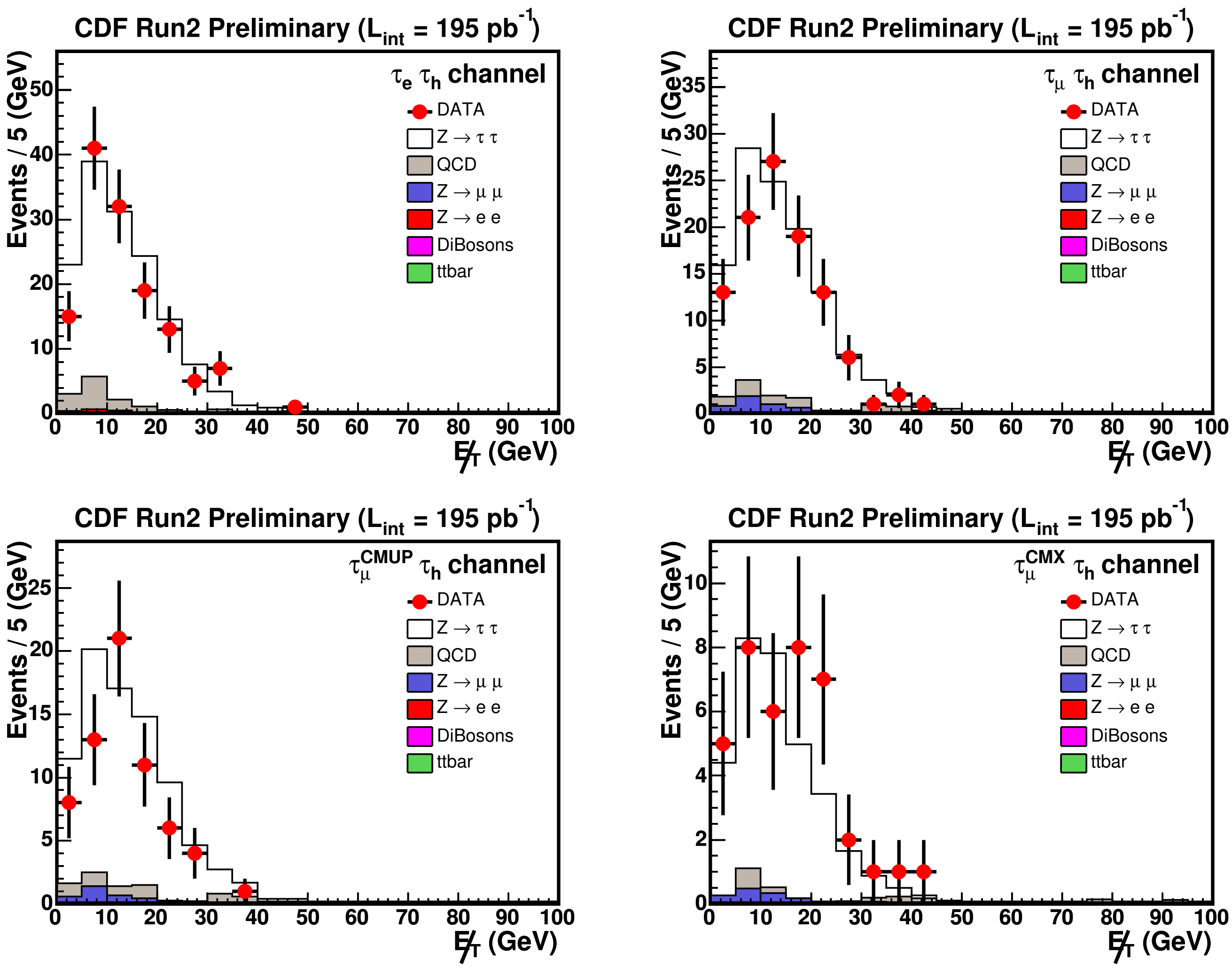

Figure 14: *Missing transverse energy in the event.*

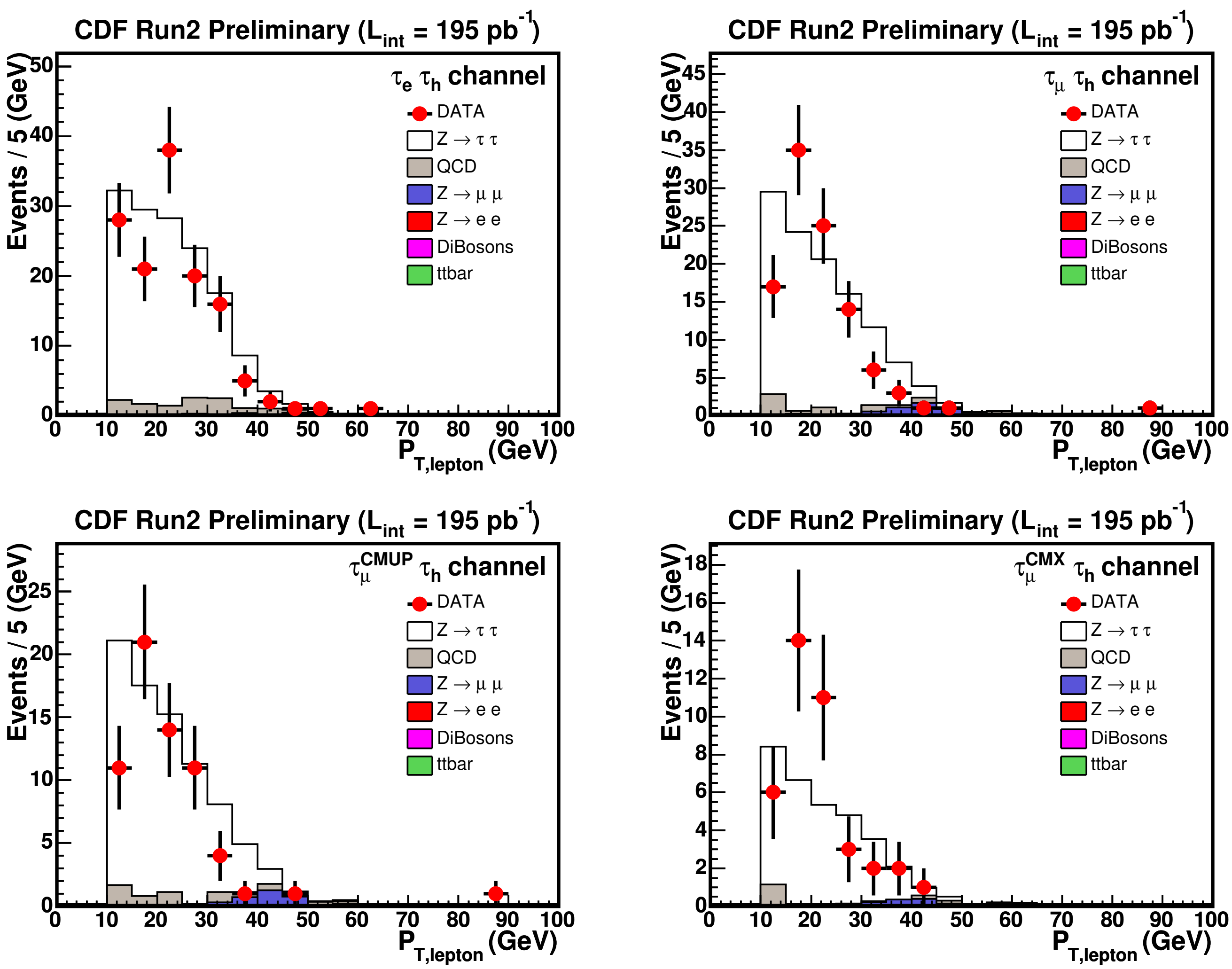

Figure 15: *Transverse momentum of the lepton.*

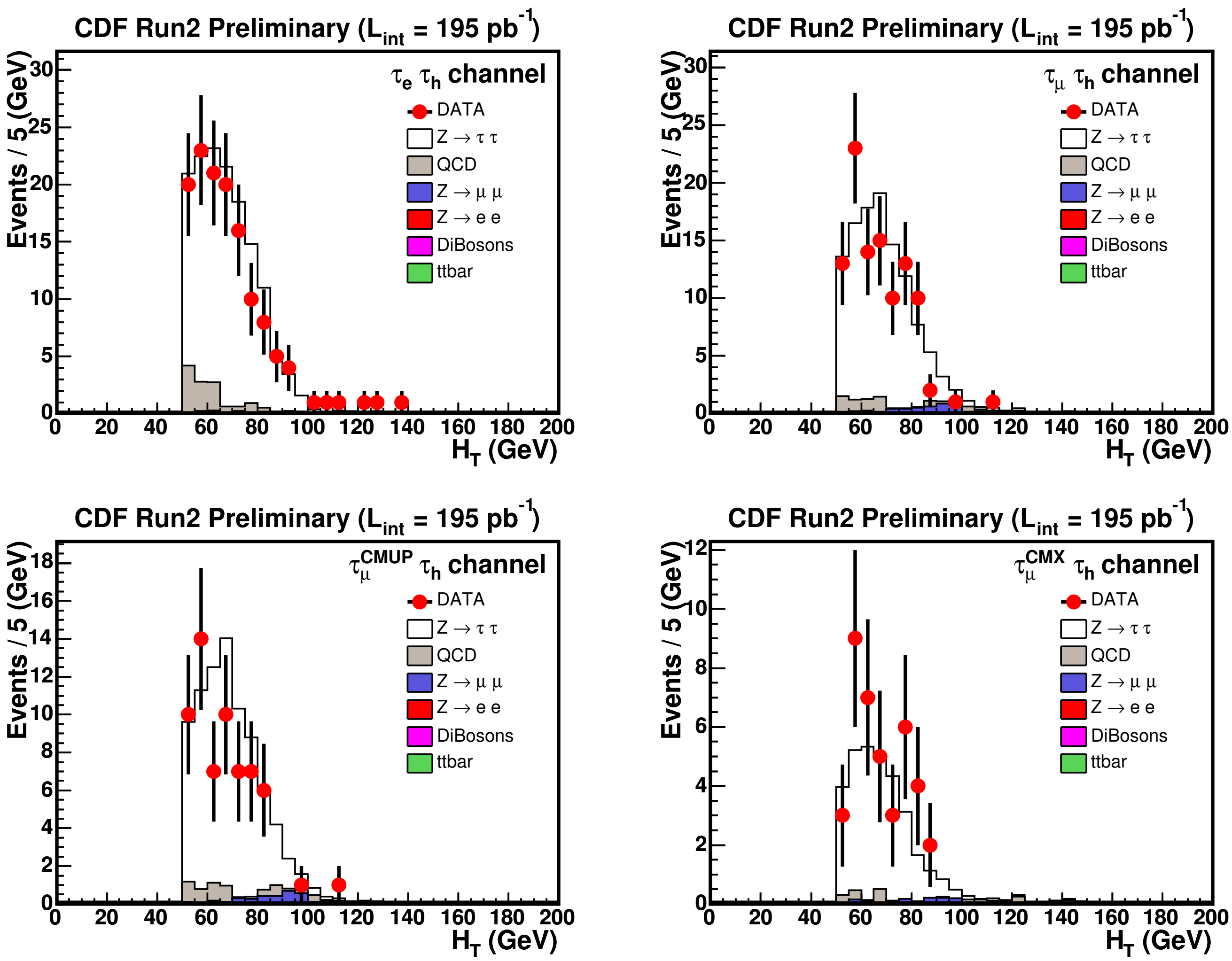

Figure 16: *Scalar sum of tau p_T, lepton p_T, and MET.*

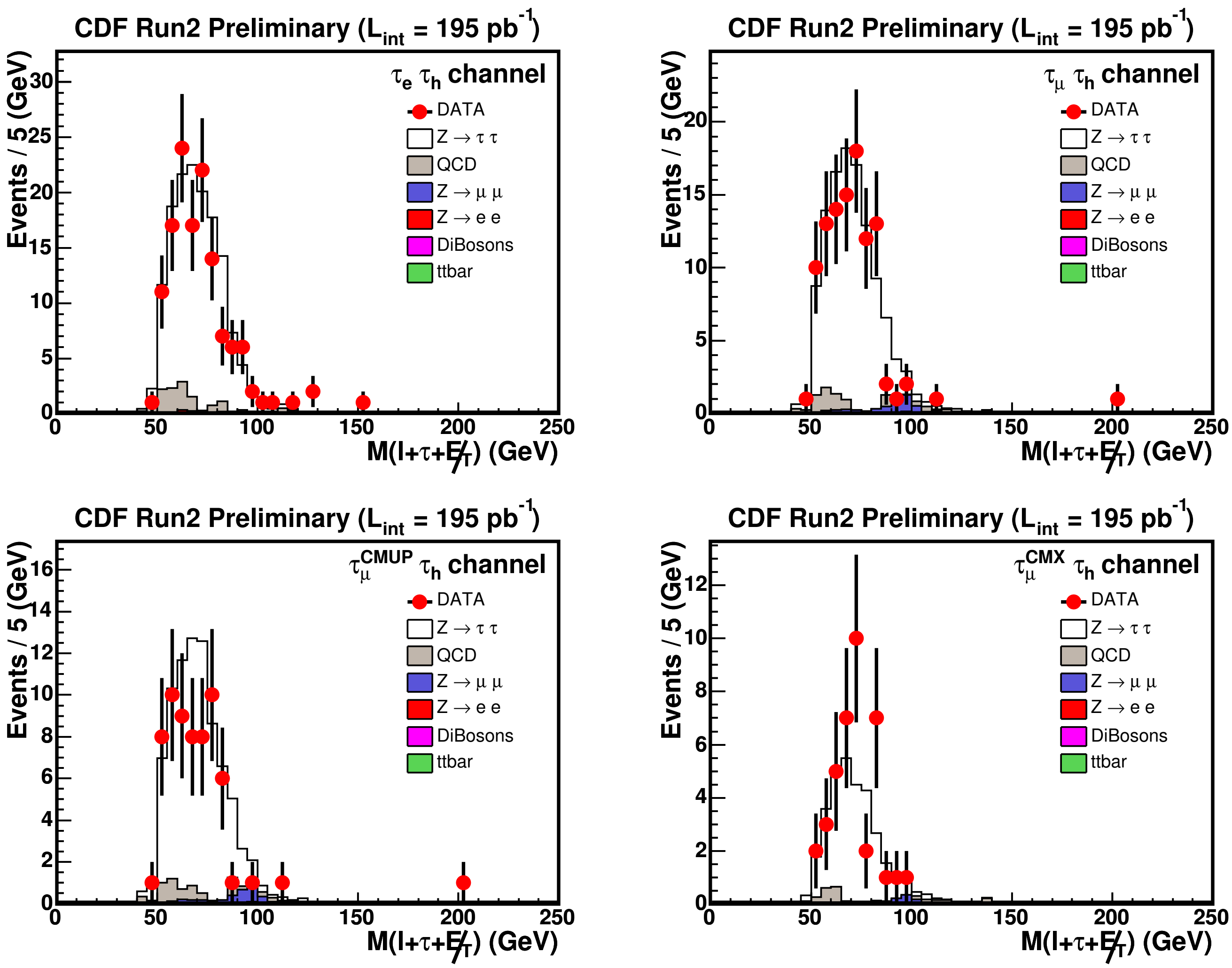

Figure 17: *Mass of lepton, tau and MET.*

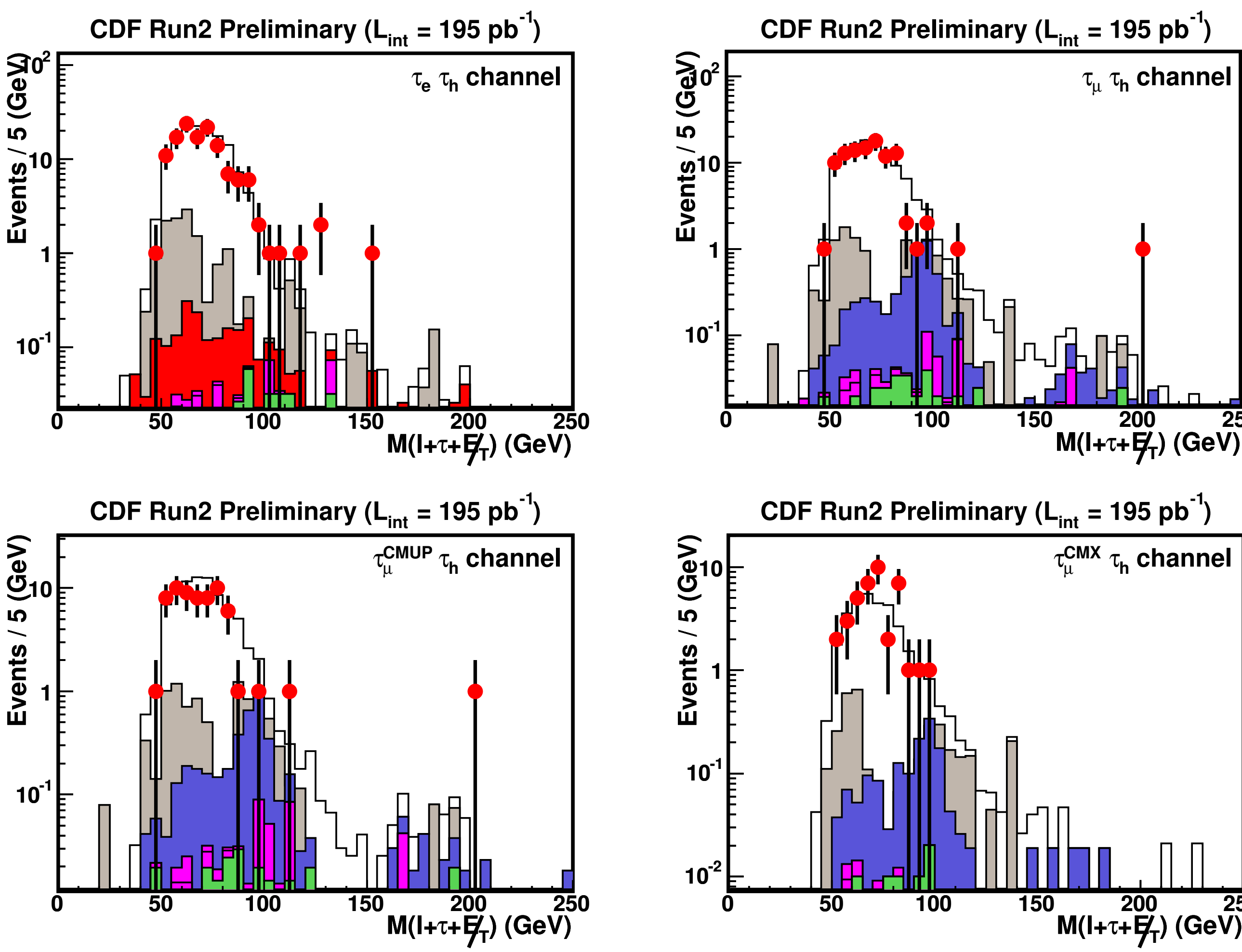

Figure 18: *Mass of lepton, tau and MET (log scale).*

9 Systematic uncertainties

There are several sources of systematic uncertainties affecting the analysis:

- Particle ID
- Event cuts
- Background estimation
- PDF functions used in MC simulation
- Luminosity
- Trigger efficiency

We rely on MC simulation to predict the particle interaction in the detector and to estimate signal efficiency and most of the backgrounds. We account for possible differences between data and MC particle ID efficiencies through the introduction of scaling factors applied to MC. The uncertainties in determining these factors are assigned as systematic errors of particle reconstruction and ID efficiency.

Deficiencies in calorimeter response simulation lead to MC/data differences in measured MET. While we do not place any direct cuts on MET, it is used in both of our event cuts. The MET-related systematic uncertainty is estimated using $\gamma + jet$ data sample. The procedure is analogous to the one used for the $Z \to \tau_e \tau_h$ cross section measurement [12]. The difference is that we use reconstructed photons instead of conversions, and chose different parametrization direction for MET. The procedure is described in Appendix E. The effect on the efficiency is estimated to be 1.0%.

The hadronic scale uncertainty affects the acceptance through the requirement on minimum tau cluster energy, calorimeter isolation cuts, the ξ cut, and tau seed tower threshold. We vary the hadronic energy by +10% and −6% and observe change in efficiency by 3%. The larger upward variation is to account for reported difference in hadronic energy deposition by single tracks between data and MC [14]. Possible energy shift in $tracks{+}\pi^0$'s energy (Appendix F) leads to 1% uncertainty in acceptance.

The systematics related to background estimation are determined by uncertainties in cross-sections for processes estimated using MC, and fake rates for $jet \to \tau$ fakes (plus statistical errors on the estimates).

Particle ID and luminosity are treated separately and are not included in these errors.

The systematic uncertainties in acceptance associated with the lack of precise knowledge of the Parton Distribution Functions (PDFs) are different for the Z backgrounds and the $Higgs$ signal. The former are estimated to be less than 3%, while the latter are substantially higher: of the order of 7.5%. Discussion of the effect of PDF uncertainties on Higgs acceptance is given in Appendix B.

We use the standard luminosity uncertainty of 6%.

Trigger systematics are taken from the trigger studies notes [13]. Additional uncertainty due to the XFT efficiency adjustment of 1.09% is added in quadrature (see Appendix D).

Table 9 summarizes the systematic uncertainties used in the analysis.

Parameter	Sys error(%)
e ID	4
μ ID	4
τ ID	10
MET	1
Hadronic energy scale	3
Trks+π^0's energy scale	1
$jet \rightarrow \tau$ fakes	30
$\sigma \times \mathcal{B}(Z \rightarrow ll)$	2.1
PDFs (Z, W)	3
PDFs $(Higgs)$	7.5
e trig	2.2
$\mu(CMUP)$ trig	1.4
$\mu(CMX)$ trig	1.4
"track" (tau) trig	1.4
Luminosity	6

Table 5: *Systematic errors used in the analysis.*

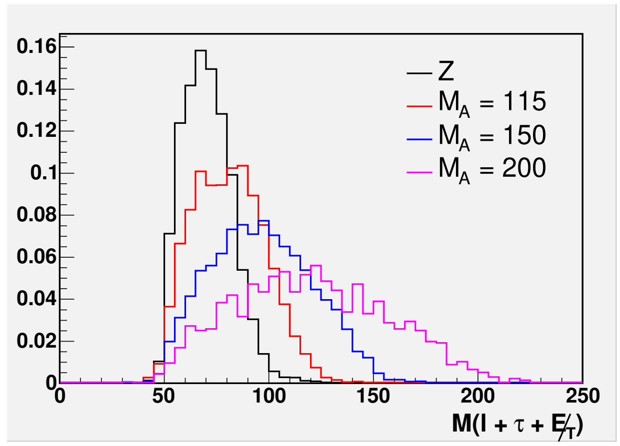

Figure 19: *Vissible mass for Z and Higgs bosons. All distributions are normalized to unit area.*

10 Results

We wish to determine the observed rate of MSSM Higgs production in our sample, and either measure a cross section (and win the Nobel Prize) or set an upper limit on its value.

The presence of neutrinos in the final state combined with lack of information on the center of mass energy and longitudinal component of the missing energy, does not allow exact mass reconstruction for Higgs bosons (or Z's) decaying to tau pairs. Instead, we use "visible mass" formed from the tau, the lepton, and missing transverse energy (treated as a four-vector). This is a mass-like quantity that allows some discrimination between Z and heavier Higgs bosons. It does not peak at the real mass of the particle and is used only as a discrimination variable. Figure 19 shows the distributions of the reconstructed visible masses for Z and Higgs bosons.

With increasing mass the separation between Higgs and Z improves (although at a slower rate). Detection efficiency also improves with mass - Figure 20. These factors work in favor of setting better limits for heavier Higgs bosons, however, the production cross sections are expected to be lower.

10.1 Likelihood

We employ a binned likelihood method using the visible mass distribution. We combine all channels in the final distribution. Then, if we observe n_i events in each bin i of m_{vis}, and we expect μ_i events from signal and background sources, we can write the likelihood as the product of the individual bin Poisson

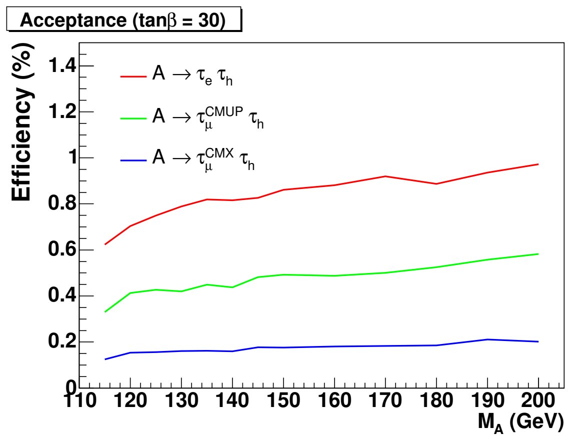

Figure 20: *Detection efficiency as a function of Higgs mass.*

probabilities:

$$\mathcal{L} = \prod_i \frac{\mu_i^{n_i} e^{-mu_i}}{n_i!} \quad (2)$$

The number expected in each bin is given by the sum over various sources, indexed by j:

$$\mu_i = \sum_j L_j \sigma_j \epsilon_{ji} \quad (3)$$

where L_j is the integrated luminosity, σ_j is the cross section, and ϵ_{ji} is the efficiency for source j. Sources include the Higgs signal, Drell-Yan backgrounds, QCD fake background, etc.

10.2 Treatment of Systematic Errors

The quantity in which we are interested is in fact the cross section for the signal, which we can take to be σ_1 for example. All other parameters in the likelihood are treated as nuisance parameters, and to the extent that they are unknown they represent systematic errors present in the analysis.

We deal with the uncertainties on these parameters by introducing Gaussian constraints into the likelihood. For example, if we let σ_2 represent the cross section of, say, $Z \rightarrow \tau\tau$ production, and we believe its value is $\sigma_2 = 254 \pm 5.4$ pb, we write the likelihood as

$$\mathcal{L} = \prod_i \frac{\mu_i^{n_i} e^{-mu_i}}{n_i!} \times G(\sigma_2, \tilde{\sigma}_2, \Delta\sigma_2)$$

where G is a gaussian function with mean $\tilde{\sigma}_2 = 254$ pb and width $\Delta\sigma_2 = 5.4$ pb.

Then the question arises as to how to treat the Gaussian constraints. There are two main methods used commonly in CDF: marginalization and profiling. In marginalization one simply integrates the likelihood with respect to the nuisance parameter:

$$\mathcal{L} = \int_0^\infty \prod_i \frac{\mu_i^{n_i} e^{-mu_i}}{n_i!} \times G(\sigma_2, \tilde{\sigma}_2, \Delta\sigma_2) d\sigma_2$$

Often one refers to this as "smearing the likelihood". This calculation is best performed by Monte Carlo integration when there are many such parameters and the integral becomes multidimensional.

In profiling, one simply maximizes the likelihood with respect to the nuisance parameters. This is typically what is done when one is making a measurement (as opposed to setting a limit). One usually minimizes $-\ln \mathcal{L}$ using MINUIT or some other function minimization package; these are very efficient and rapid to use.

We choose the profiling method here. In the CDF Statistics Committee, studies have indicated that for complex problems such as a binned likelihood fit, the two approaches give indistinguishable results. [15]

10.3 Non-Gaussian Constraints

There can be in addition parameters that encode other systematic errors other than those appearing in the equations above. Most enter as multiplicative factors; for example the data/MC scale factors for lepton and tau ID multiply the appropriate terms in the μ_I. Other factors lead to a net "smearing" of the signal cross section and are treated by an overall additive term applied to the signal cross section.

A more detailed discussion of these sorts of systematic error parameters appears in the note on the t' search [16]. There it is pointed out that the techniques described here only work in the case where the errors are reasonably small, less than about 20%. For larger errors the Gaussian terms tend to cause the likelihood to reach an asymptotic minimum at some value as the signal cross section increases. This means that the integral of the likelihood diverges, and one cannot set a limit using the usual Bayesian method of finding the cross section beyond which 5% of the likelihood integral lies.

This divergence is present in this analysis due to the large uncertainty in the Higgs cross section that would result from a tau energy scale shift of 2%, in the case where we represent it by an additive parameter which has a Gaussian constraint. The reason is that the width of the Gaussian constraint is quite large for this magnitude of a tau energy shift, especially for the smaller Higgs masses.

A typical example of this shift as a function of cross section is shown in figure 21 for one mass point. The plot shows the average deviation in the observed cross section one expects as a function of the true Higgs cross section, as estimated from pseudoexperiments ion which a Higgs signal was generated, along with the other backgrounds, based on distributions of visible mass where the tau energy scale was shifted upwards by 2%. In each pseudoexperiment, then the Higgs cross section was measured using the normal unshifted distributions.

As in the t' analysis, the question immediately arises as to whether a Gaussian truly represents what we believe about the uncertainty. As discussed above we believe that the assigned uncertainty of 2% on the energy scale represents more of an upper limit on the possible shift in tau energy scale, as opposed to a 1-sigma Gaussian uncertainty. Thus, following the example of the t' case, we utilize a non-Gaussian constraint of the form

$$Q(\Delta\alpha) = \frac{e^{(-2\Delta\alpha^4/\sigma_\alpha^4)}}{\sigma_\alpha} \tag{4}$$

Here $\Delta\alpha$ represents the deviation in the additive parameter from zero. This function has a flatter shape in the central region, and cuts off rapidly beyond $\Delta\alpha = \sigma_\alpha$.

10.4 Expected Sensitivity

We have estimated the sensitivity of the analysis for luminosity 195 pb^{-1} (electron + muon channels) by performing pseudo-experiments.

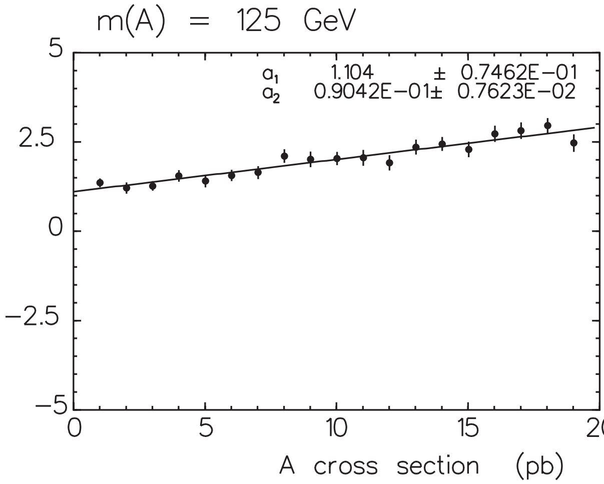

Figure 21: Average shift in apparent Higgs cross section due to 2% tau energy scale shift, as a function of true Higgs cross section, estimated from pseudoexperiments as described in the text.

mass (GeV)	upper limit (pb)
115	19.03
120	11.43
125	9.76
130	9.00
135	7.83
140	7.19
145	6.15
150	5.71
160	4.84
170	3.80
180	3.48
190	2.84
200	2.55

Table 6: Upper limits at 95% CL on MSSM Higgs cross section times branching ratio to tau pairs as a function of Higgs mass.

10.5 Upper Limits on Higgs Cross section

We perform the procedure described above to each of the hypothetical Higgs mass points, and, seeing no evidence of a signal, calculate 95% CL upper limits on the cross section times branching ratio of Higgs production in the sample.

Table 6 shows these limits as a function of the Higgs mass, and Figure 22 shows a plot of the limits versus Higgs mass, together with the predicted limits from the pseudoexperiments.

These limits can (and will) be interpreted in the space of $m(A)$ versus $\tan\beta$ of the MSSM - this work will be completed soon and combined with the high mass search.

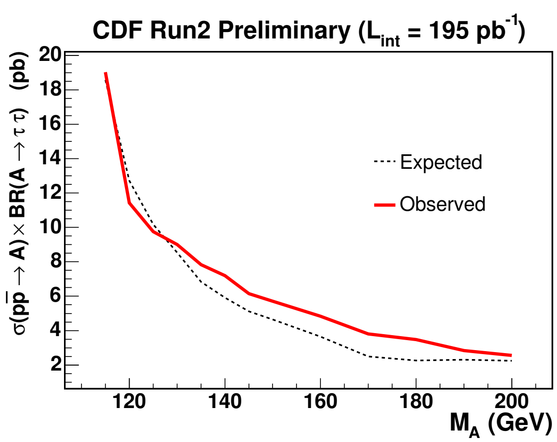

Figure 22: *Expected and observed limits for A production ($\sigma \times BR(A \to \tau\tau)$).*

References

[1] Report of the Tevatron Run 2 Higgs Working Group, hep-ph/0010338.

[2] A. Connolly, CDF note 6806.

[3] S. Baroiant *et al.* "Update on the Lepton+Track Trigger in Run II - Definition and Physics Goals", CDF6325 (2003).

[4] M. Coca, E. Halkiadakis " Central Electron Identification Efficiencies for the 200 pb^{-1} Run2 Dataset", CDF6580 (2004).

[5] V. Martin, L. Cerrito "Muon Cuts and Efficiencies for 4.11 Analyses", CDF6825 (2004).

[6] Anton Anastassov *et al.* "Tau Reconstruction Efficiency and QCD Fake Rate for Run 2", CDF6308 (2003).

[7] Fedor Ratnikov, "Tau Reconstruction for CDF Run 2", CDF6252 (in preparation).

[8] Anton Anastassov, "Non-isolated π^0/γ Reconstruction", CDF6688 (2003).

[9] Colin Jessop, "A Search for the Top Quark Decaying to the Charged Higgs Boson in $p\bar{p}$ Collisions at $\sqrt{s}$ = 1.8 TeV", PhD Thesis, Harvard University (1993).

[10] J. Conway *et al.*, "Tau Identification", CDF3545 (1997).

[11] http://www-cdf.fnal.gov/internal/physics/exotic/tau/

[12] S. Baroiant *et al.* "$Z^0 \rightarrow \tau\tau$ Cross-Section Measurement", CDF6552 (2004).

[13]

[14] Pasha Murat, Talk given at the Simulation Meeting on July 31, 2003.

[15] See John Conway's presentation from the February 2004 CDF Statistics Meeting, available on request.

[16] R. Erbacher *et al.*, "Search For t' In High-p_T Lepton Events", CDF6888 (2004).

A Fake Rate Measurement and Consistency Checks

Using JET 20, 50, 70, 100 samples we have determined corresponding estimates of the fake rates to be used in QCD background determination. We are interested in *relative* fake rates as defined in Section 6. We used "minimal" parametrization in terms of E^{cl} and η_{det}. Attempts for trigger bias removal as described in Section 6 did not lead to consistent results. While the estimates from JET50, 70, 100 are quite similar, JET20 yields substantially higher fake rates. It is especially disturbing that the discrepancy is most pronounced in the region $20 < E_T^{cl} < 40$ GeV, where most of our tau candidates are expected to reside.

Discrepancies in fake rates obtained from the different jet samples would not come as a surprise to people who make use of the fake rate method. We have observed this problem and reported on it in a previous note [6]. Run 1 analysis have observed similar behavior [10].

In most cases there is no clear indications on which prediction should be used. One usually taken approach is to use the average of all predictions as a central value and assign the differences with the individual predictions as systematic errors. We have used it ourselves, but never felt comfortable with the accompanying large systematics (even if they have small impact on our results).

It would be nice to understand the source of the inconsistency and come with a global solution to the fake rate problem. While this is worked on, we are satisfied to take a purely pragmatic approach.

The sources contributing to the $jet \to \tau$ backgrounds were listed in Section 7.4. We identify three independent samples that allow testing of the fake rate predictions of the jet samples against the actual number of observed events. The source are examined separately to account for possible jet property differences.

- n-jet sample passing event cuts:
  Non-isolated leptons (or lepton fakes) selected by removing the calorimeter isolation and reversing the track isolation cut s for the lepton (e, μ). Event cuts are applied without modification.

- $W + jet(s)$:
  select control region in the $P_\zeta \; vs \; P_\zeta^{vis}$ plane as indicated on Figure **??**. Obviously the ζ cut is replaced, however, this should have no effect on the jet properties.

- $\gamma + jet(s)$:
  Relevant only for $\tau_e \tau_h$ channel, represents the source of background events with an electron from non-removed conversion (probably with one very soft leg). All event cuts applied as for signal, photon is used as replacement for the electron.

To ensure clean testing environment we place emphasis on avoiding both tau contamination and backgrounds cross-contamination in the samples.

The results of the comparisons of observed and predicted number of fakes are shown in tables below.

Sample	N_{obs}	N_{pred}^{JET20}	N_{pred}^{JET50}	N_{pred}^{JET70}	N_{pred}^{JET100}
$\gamma + jet$	748	1756.3±20.4	873.9±10.4	922.7±11.1	956.1±11.4

Table 7: *Comparison of observed fake taus with predictions for the $\gamma + jet(s)$ control sample.*

Sample	N_{obs}	N_{pred}^{JET20}	N_{pred}^{JET50}	N_{pred}^{JET70}	N_{pred}^{JET100}
TAU_ELE	20	31.7±2.3	18.2±1.3	18.7±1.4	19.0±1.4
TAU_CMUP	17	26.7±2.0	15.7±1.2	15.8±1.2	16.5±1.3
TAU_CMX	7	11.1±1.3	6.7±0.8	6.7±0.8	6.9±0.8
Total	46	69.5±3.3	40.6±1.9	40.2±2.0	42.4±2.1

Table 8: *Comparison of observed fake taus with predictions for the $W + jet(s)$ control region.*

Sample	N_{obs}	N_{pred}^{JET20}	N_{pred}^{JET50}	N_{pred}^{JET70}	N_{pred}^{JET100}
TAU_ELE	580	1308.7±16.9	620.1±8.0	653.5±8.6	666.5±8.8
TAU_CMUP	381	800.4±12.7	387.8±6.1	401.7±6.5	406.0±6.6
TAU_CMX	172	367.5± 8.6	179.1±4.1	188.0±4.5	188.4±4.5
Total	1133	2476.6±22.8	1187.0±10.9	1243.2±11.7	1260.8±11.9

Table 9: *Comparison of observed fake taus with predictions for the di-jet/multi-jet control sample.*

The conclusion that we draw from these tables is that the predictions from fake rates determined using JET50,70,100 better describe the observations in the tested samples. This may or may not be the case for other environments, but as far as this analysis is concerned, we see no justification to include predictions based on fake rates from JET20. It should be noted that JET50,70,100 are not in perfect harmony,and the best we can do is take the average of the predictions from these samples.

When determining the "final" fake rates, we include additional parametrization in terms of track multiplicity. Due to the low statistics, we apply a smoothening procedure for the results and use the resulting continuous function in our predictions. The first order of business after making such a step is to perform a sanity check. Regardless of how the function is constructed, its fitness can be determined by going back to the original JET50,70,100 samples and comparing the observed and predicted distributions for the input parameters E^{cl}, η_{det} and N_{trk}. This comparison is shown in Figure A. There is a good agreement between the prediction and the observed events. Regions exhibiting some deviations are not unexpected - the fake function is constructed to describe the "averaged" fake rate, and will highlight differences between the samples. Our conclusion is that the function provides satisfactory description of the samples and we can use it in our estimates.

The real test of the QCD prediction is performed on the control samples described above. We review the predictions for the variables used in the parametrization, as well the predictions for the effective mass. The latter is of special importance for the analysis, because it is the variable used in the limit extraction. The effective mass comparison is made between predicted and observed distribution involving $jet \rightarrow \tau$ fakes. The shape of the distributions should not be compared with the expectation in our final sample [6].

The comparisons are presented below. We see a good agreement for all distributions and samples. As an additional test (mostly to satisfy our curiosity) , we compare the predictions and observations when applying the fake rates to a MC sample of $W \rightarrow e\nu + jet(s)$. The benefit of using this MC sample is that we can get an idea about the effective mass shape in our signal region (however, $W \rightarrow e\nu + jet(s)$ is a small fraction of the fake tau backgrounds) . We were a little sceptical about the performance of the fake rate function for MC, but the results turned out to be a pleasant surprise.

The observed distributions give us confidence in the prediction of the effective mass shape for $jet \rightarrow \tau$ fakes. The predicted number of fakes taus is well contained in an interval of $\pm 20\%$ of the observation. This is assigned as uncertainty in the estimated fake rates.

[6] This is especially true for $W + jet(s)$ sample selected from data. In this case the topology is quite different from our signal due to redefinition of the ζ region.

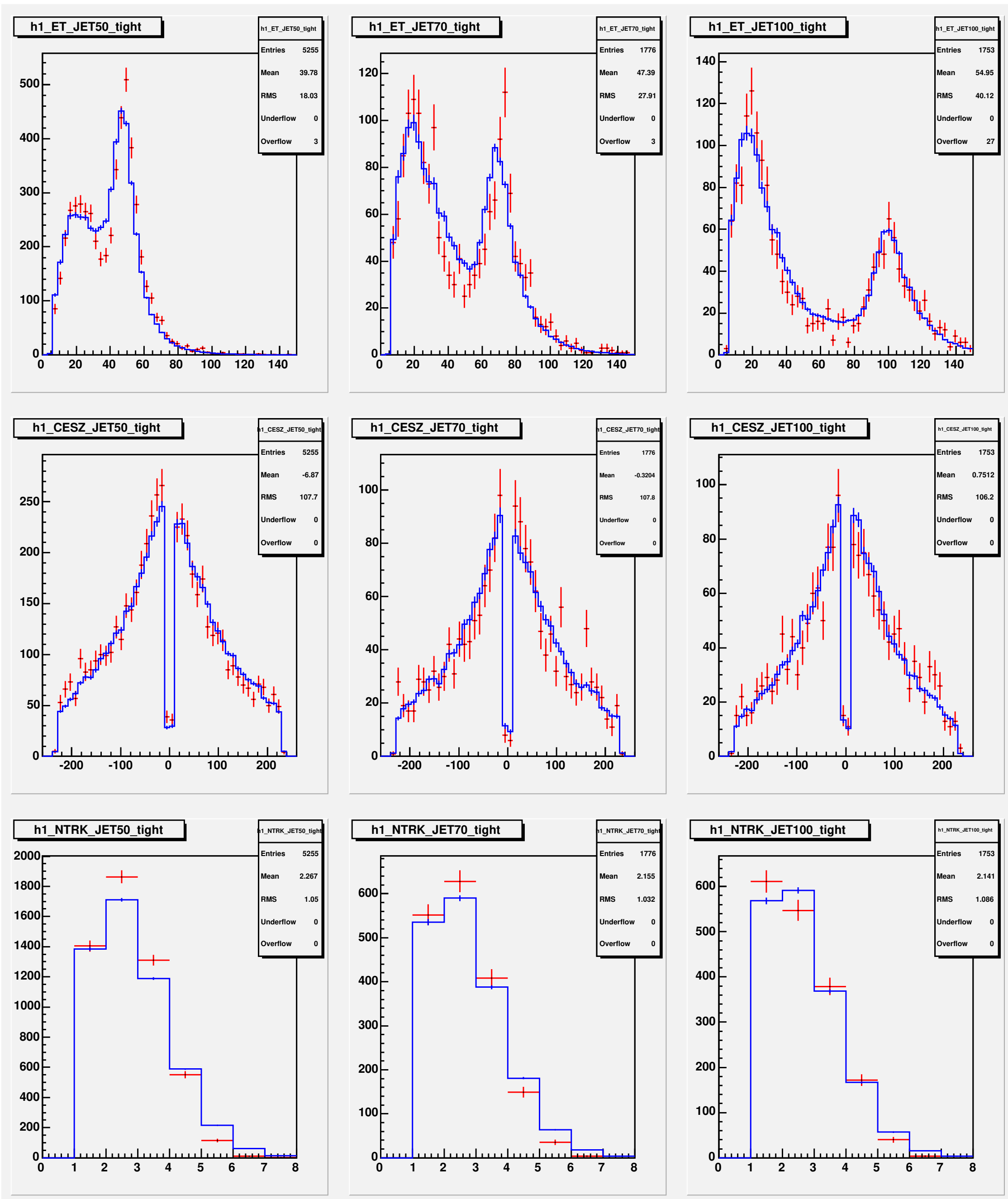

Figure 23: Comparison between predicted (blue histogram) and observed $jet \rightarrow \tau$ fakes (red points with error bars) for JET50,70,100 as indicated.

$\gamma + jet$ control sample

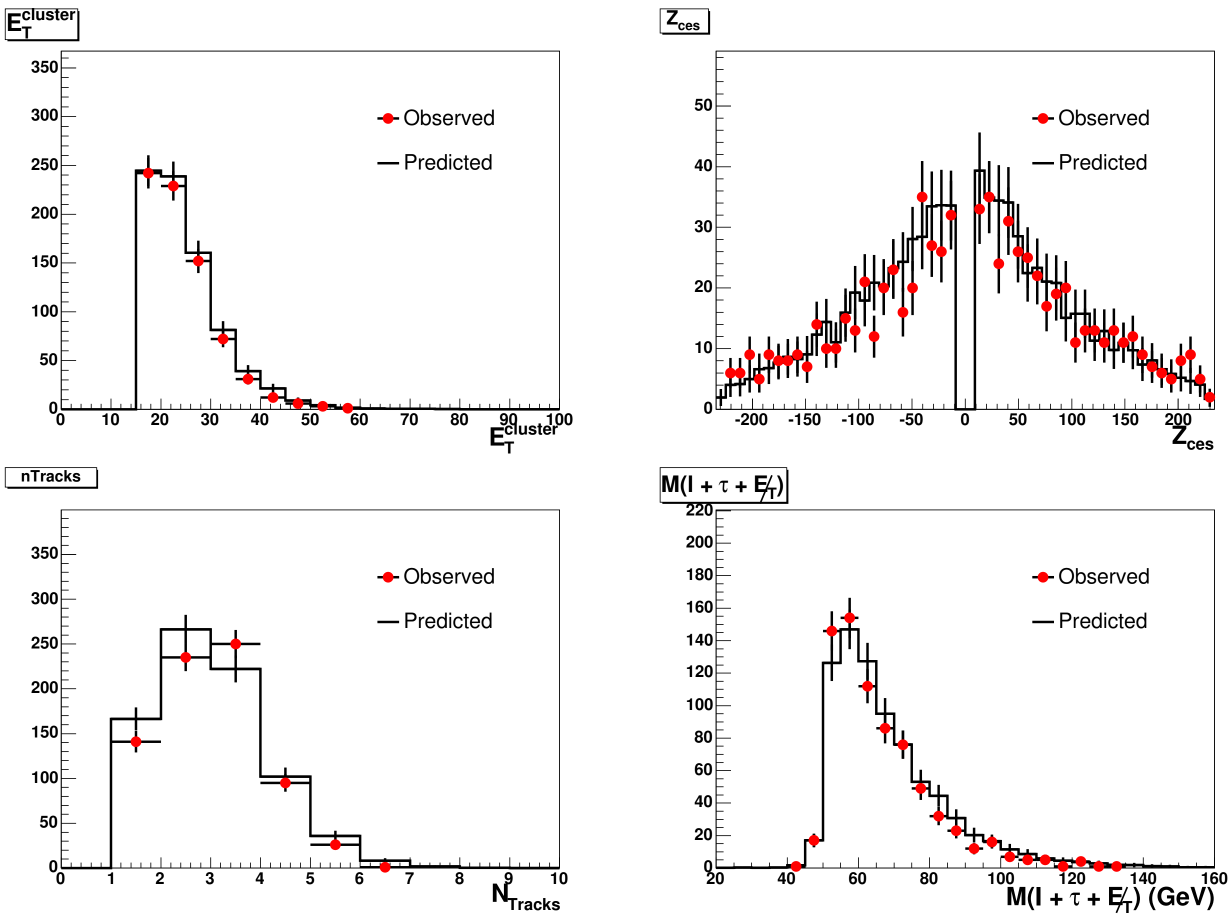

Photon energy and direction is used in place of the electron for the calculation of effective mass.

QCD control sample

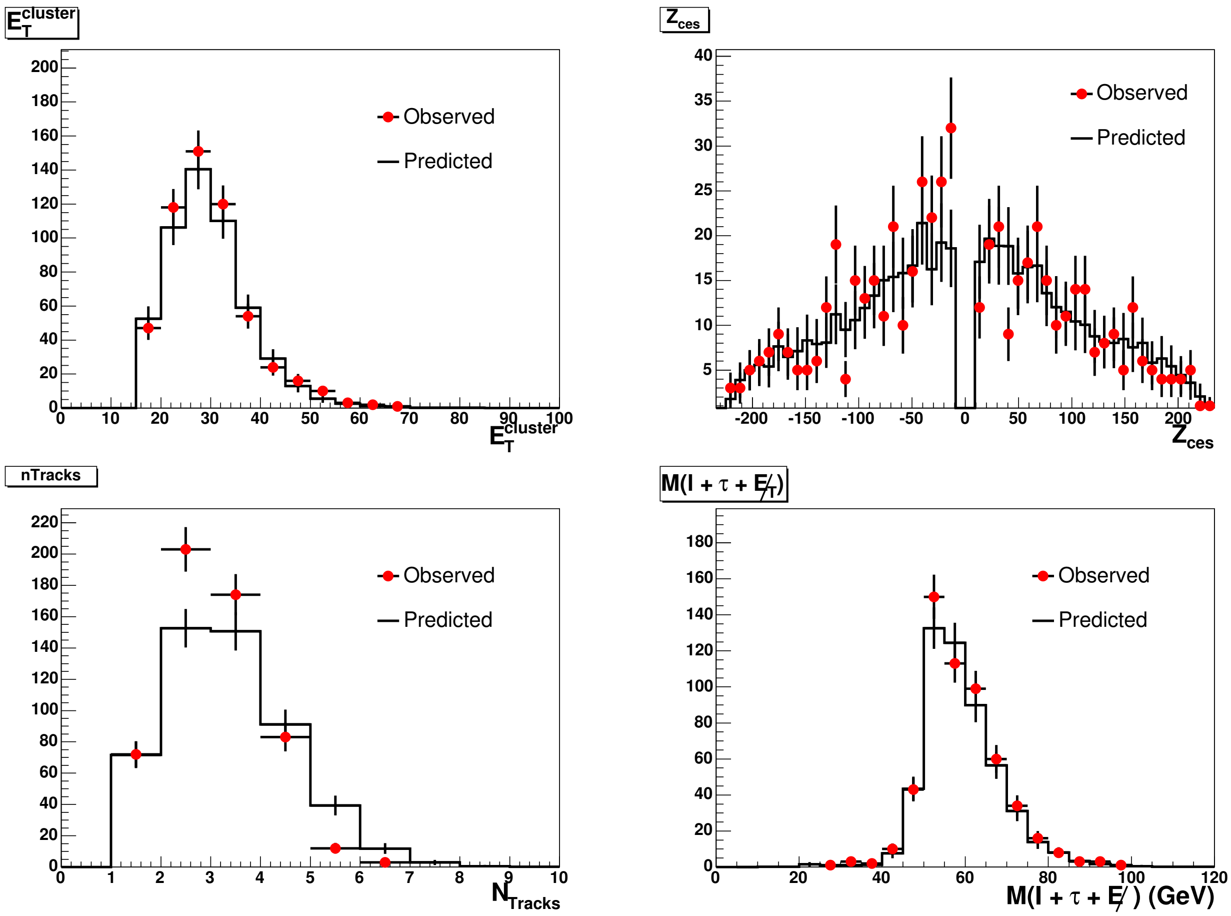

$W + jet(s)$ sample from control region in zeta plane

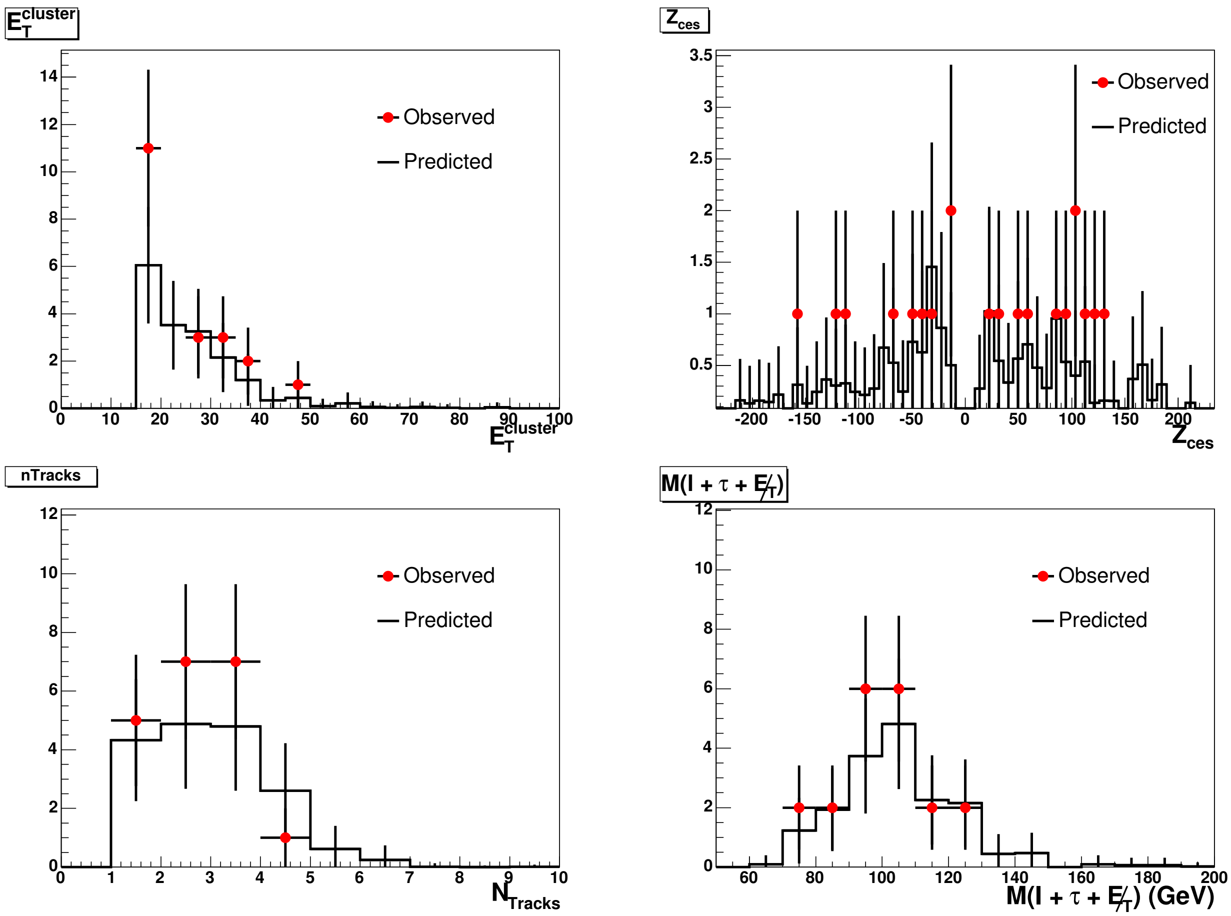

$W + jet(s)$ MC with all event cuts applied.

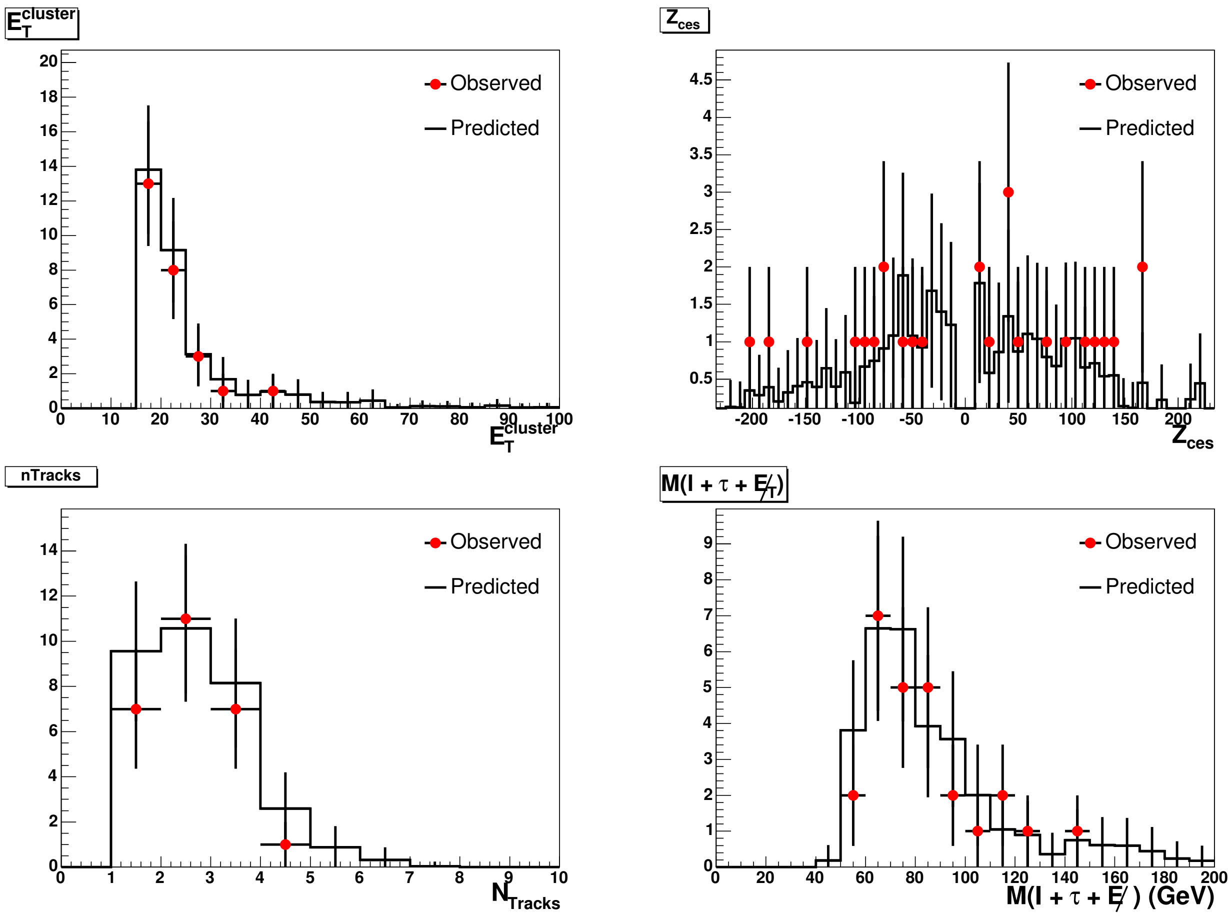

B PDF Systematic Error

The Parton Distribution Functions (PDFs) are not precisely known, and this uncertainty leads to a corresponding uncertainty in the predicted cross sections, as well as the acceptance. We are mainly interested in how the acceptance varies with varying PDFs. The proper way to carry out this study — generating separate sets of Monte Carlo events for each PDF set one wanted to investigate – would be prohibitive. Instead, we follow the prescription advocated by the Top Quark group[7] and reweight the same set of generated events with different PDF sets, and observe the cross section and acceptance changes.

The MSSM higgs production process is relatively sensitive to the PDFs. The production proceeds via $b\bar{b}$ annihilation and therefore depends on the sea-quark distribution of the proton.

B.1 Variations due to CTEQ5, CTEQ6

We use Pythia 6.216 for all our Monte Carlo generation, which uses CTEQ5L PDFs. We investigated 41 CTEQ6 eigenvectors. We report the differences between CTEQ6L and CTEQ6L1, and between CTEQ6M (NLO) and CTEQ5L (LO).

The weights are calculated for each event using the HEPG 4-vectors, and the Q^2, which we set to M_A^2. [8]

We calculate the acceptance by requiring the visible decay products of the τ to have $|\eta| < 1.1$, and then require the sum of energies of these particles to be greater than 10 GeV.

Figure24 shows the acceptance changes vs. M_A for various ratios of CTEQ and MRST PDFs. We see that largest change in acceptance, about 4%, happens when comparing the CTEQ5 to CTEQ6 schemes, and also when comparing the CTEQ5 to MRST72. We estimate a 4% systematic error due to the CTEQ5,6 differences and another 4% due to CTEQ5 vs. MRST72 differences.

B.2 Variations due to α_s

Another significant source of PDF uncertainty is the variation in α_s. Other analyses, including several top-quark analyses have used the difference between MRST72 and MRST75 [9] to determine the systematic due to α_s uncertainty.

However, we find we cannot use these distributions to determine $A \to \tau\tau$ acceptance systematic error.

An increase in α_s leading to more gluons and b would increase the cross section. A change in the x distribution would lead to a change in acceptance, as the decay became more or

[7] Stephen Miller, private communication

[8] Varying the Q^2 scale does not affect the results significantly.

[9] This schema refers to MRST LO central gluon and MRST LO lower α_s from Eur. Phys. J C4 (1998)

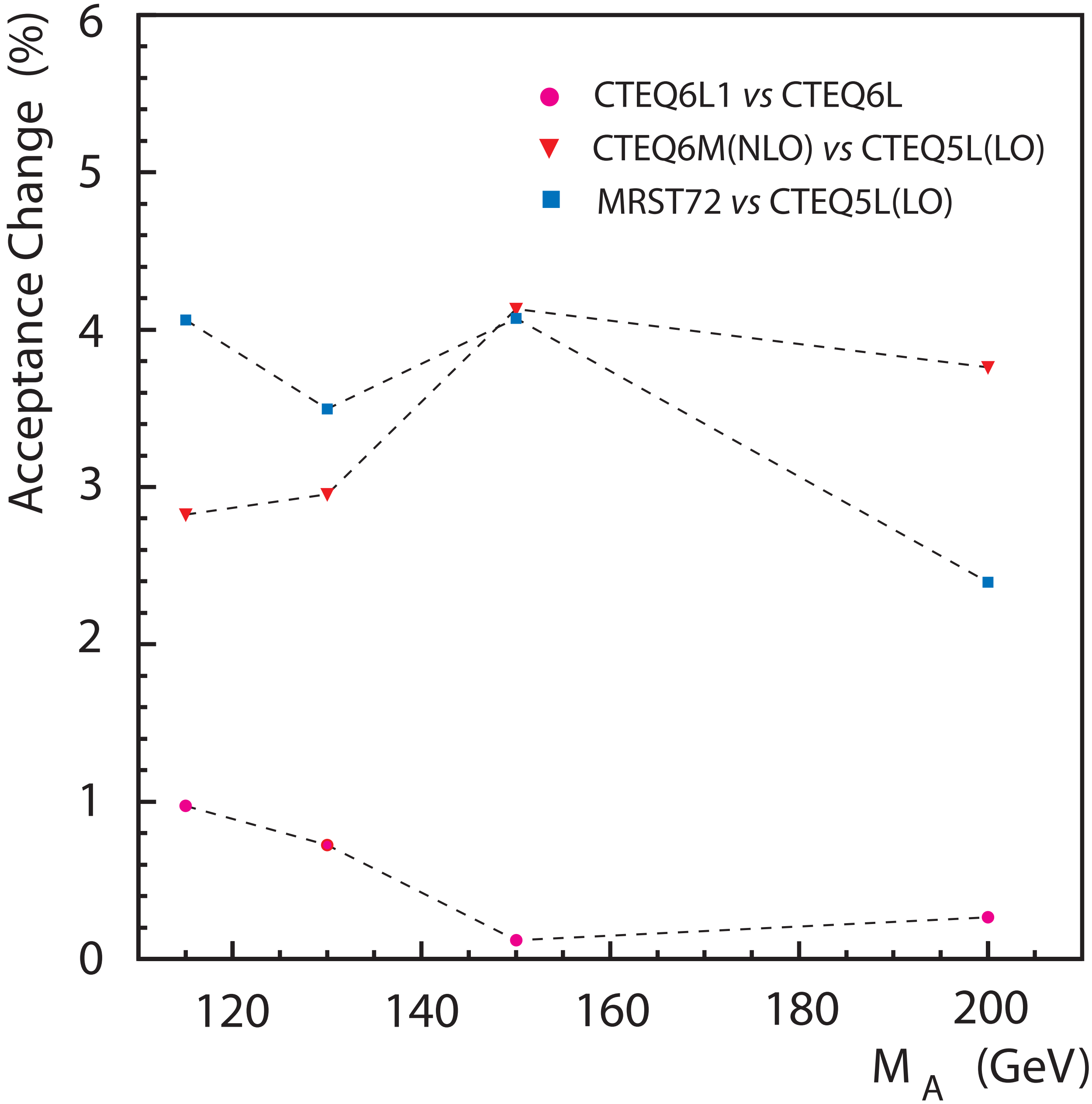

Figure 24: Acceptance variations comparing various PDF distributions. The Monte Carlo used is 1000 events of $A \rightarrow \tau\tau$, at various masses, and $\tan\beta = 30$.

less forward. In top production, the uncertainty in the acceptance is typically a factor of 5 lower than the uncertainty in the cross section.

However, in the MRST72 to MRST75 comparison, a typical cross section difference (for $M_A = 115$ GeV/c^2, $\tan\beta = 30.$) is approximately 8%, but the acceptance difference is 12%. The b-quarks and gluons that produce the A come from the proton sea distribution which is peaked at low values of x. Comparisons of the MRST72,75 x distributions for b-quarks showed a significant change at higher x, which causes the change in acceptance. However, it seems unlikely that the change in acceptance would be larger than the change in cross section.

B.2.1 Newer Schema for MRST

This section is entirely the work of Joey Huston. We (well, actually Joey Huston) suspected the MRST PDF distributions, and investigated the MRST2001 (NLO) distributions. In comparing to CTEQ6.1 (also NLO), we find the b-quark distribution is ∼10% lower than the central MRST2001 b-quark distribution which means that the cross section would be ∼20% lower.

There was not much difference for the lower and higher α_s predictions in the Q^2 range of interest, contrary to what we found with the 1998 MRST.

Taking the example of top quark production where the acceptance difference is a factor of 5 smaller than the cross section difference, we put a 5% systematic error due to α_s variation.

B.3 Final PDF Systematic

We estimate the systematic uncertainty due to PDF as follows: 4% due to CTEQ5,6 differences, 4% due to CTEQ5 vs. MRST72, and 5% due to α_s variation. We add these three in quadrature and get a 7.5% systematic uncertainty due to PDF. This is larger than most other analyses because A production depends on b-quarks from the proton sea.

C Tau Efficiency Scaling Factor

For now we use absolute normalization of reconstructed taus from $W \to \tau\nu$ in the data and MC to determine the data/MC scaling factor for tau efficiency. Absolute normalization allows determination of the combined effect of all selection criteria.

The scaling factor S_τ is defined as

$$S_\tau = \frac{\epsilon(data)}{\epsilon(MC)} = \frac{N_\tau(data)}{N_\tau(MC)},$$

where $N_\tau(data)$ is the measured number of taus in the data sample passing all tau cuts (corrected for backgrounds), and $N_\tau(MC)$ is the corresponding number of reconstructed taus in the MC scaled to luminosity and measured $\sigma(p\bar{p} \to W) \times BR(W \to l\nu)$ (lepton universality is assumed).

The sample used to determine the data/MC scaling factor is selected with the TAU_MET trigger and corresponds to $L_{int} = 72\,pb^{-1}$. To select a tau sample with high purity, we require one tau candidate with $P_T > 25$ GeV and apply tight event cuts: $\not{E}_T > 30$ GeV, no extra jet with $E_T > 5$ GeV (cone 0.7). The extra jet veto requires $W \to \tau\nu$ MC to be rescaled to account for proper fraction of events with no jets. The scaling factor was obtained from comparison $Z \to \mu\mu$ data and MC and was determined to be 0.853 ± 0.022 (see CDF7026).

Most of the backgrounds are from Z/W decays and are obtained from MC. The estimate of the $jet \to \tau$ fakes using the method described in the note returned results consistent with no jet backgrounds. As an alternative, we used a fit of the track multiplicity distribution in data (after correcting for all Z,W backgrounds) with shapes expected for tau (taken from MC) and jets (from JET20, 50, 70) samples. There was no significant difference between the results from different jet samples [10].

We take the average of the scaling factors with the two estimates of QCD (no QCD and QCD from the shape fit) as the central value. The difference between the central value and the two estimates is included in the uncertainty of the scaling factor. The scale factor is obtained for 1- and 3-prong tau candidates with $|Q| = 1$. The number of data events after subtraction of W, Z backgrounds is 558.3 ± 25.2. The multiplicity shape fit (taken as the high limit for QCD) predicts 35.7 ± 10.5 $jet \to \tau$ fakes. The MC expectation is 572 events. The resulting scaling factor is 97.6% with no QCD, and 91.3% with QCD estimated from shape fitting.

The average is $S_\tau = 0.95 \pm 0.09$. The error is dominated by 6% luminosity uncertainty and the statistical error in the data sample 4.6%. The assigned error due to QCD uncertainty is 3.2%. The uncertainties in the W,Z backgrounds estimation and the monojet correction are small, but also taken into account.

[10] This is not surprising: in a previous note [6] we have shown that the multiplicity shapes for tau fakes obtained from these samples are consistent.

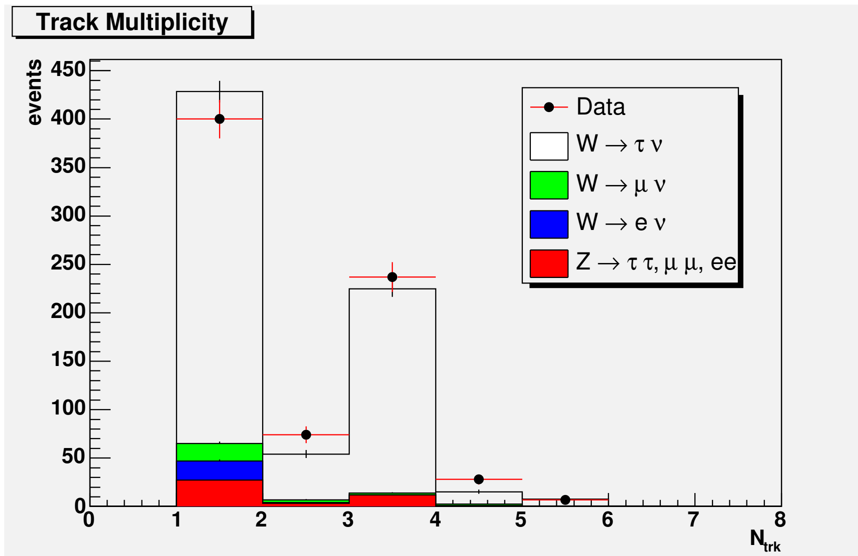

Figure 25: *Track multiplicity for tau candidates in the sample before scaling. The plot shows the data, signal from* $W \to \tau\nu$ *MC, and the W/Z backgrounds.*

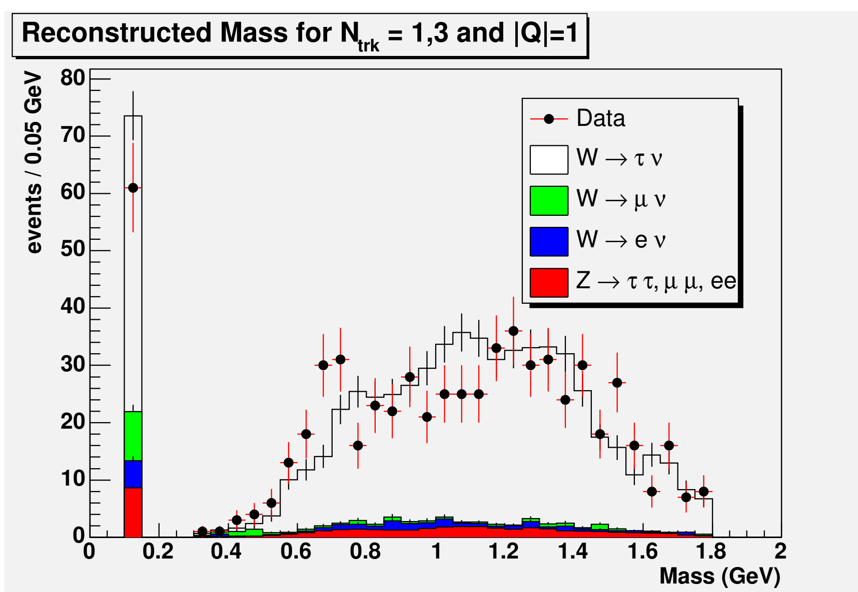

Figure 26: *Mass of tau candidates (1- and 3-prong entries only)*

D Accounting For Trigger Efficiency Effects from XFT Changes

The requirements for the XFT part of the trigger changed slightly during data taking. A detailed report of the changes and the their effects on the efficiencies can be found in CDF Note 6234. In this note, the data is broken down into 6 separate periods, and the XFT efficiency is calculated separately for each period.

The trigger efficiency used in this analysis is documented in CDF note 6257, 6358. The data used in these studies came from Periods 1 - 3 as defined in note 6234. Therefore, we do not (re)correct for the XFT efficiency in these ranges.

From Table 9 in CDF note 6234, we determine that the XFT efficiency for Periods 1 - 3 was 97.0 %. We correct as follows:

- Periods 1,2,3: 1.0 (by definition)
- Period 4: 96.4/97.0 = 99.4
- Period 5: 96.0/97.0 = 99.0
- Period 6: 94.7/97.0 = 97.6

The error incurred in calculating the XFT scale factors are small. The majority of the XFT changes, including going from requiring 4 superlayers to 3, and 10 hits to 11, as well as the turning off of a section of one superlayer, all occurred within Periods 1 - 3.

The luminosity weighted difference between Periods 4 - 6 and the Periods 1 - 3 is 1.09%. We take this as a systematic error on the XFT efficiency scales.

E Effect Of Data/MC $\not\!\!E_T$ Measurement On Acceptance

The effect of instrumental $\not\!\!E_T$ on signal selection is estimated by comparing the $\not\!\!E_T$ observed in $\gamma + jet$ data (cph108) event to $Z \rightarrow \tau_e\tau_h$ MC events. The neutrino contributions to the measured $\not\!\!E_T$ in the MC was subtracted. After the subtraction, both the "residual" $\not\!\!E_T$ in the MC sample and $\not\!\!E_T$ in the data sample measure similar activities in the detector. The $\gamma + jet$ events are selected by requiring one good photon with $E_T > 15$ GeV (passing photon baseline cuts) and a jet passing the tight tau ID cuts as defined in this Note. This creates an environment as close as possible to the $Z \rightarrow \tau_e\tau_h$ MC. The electron and the photon candidate have similar energy resolutions. We expect the tau-like jet to emulates the hadronically decaying tau in the MC. For the given event topology and a perfect detector the measured $\not\!\!E_T$ should be centered at zero. We expect possible $\not\!\!E_T$ bias due to energy mismeasurement to appear in the direction of the tau (and tau-like jet). Therefore we define parallel ($\not\!\!E_T^{\parallel}$) and perpendicular ($\not\!\!E_T^{\perp}$) components of $\not\!\!E_T$ with respect to this direction.

Figure 27 shows the distributions for the parallel and transverse components of $\not\!\!E_T$. The difference between data and MC is small. We use the mean and widths observed in data to reweight $\not\!\!E_T$ in MC.

The event cuts are applied after $\not\!\!E_T$ reweighting and the efficiency is compared to the one obtained without the reweighting procedure. The differences are taken as estimates of the systematic error due to $\not\!\!E_T$ measurement effects. The

In principle, the $\not\!\!E_T$ resolutions will depend on $\sum E_T$ of the event. Energy of electromagnetic objects (photons, electrons, isolated π^0's, etc) is measured quite well. There is a well established procedure to correct $\not\!\!E_T$ for contributions from muons. In events dominated by a tau (or tau-like jet) and a lepton or photon, the most important factor will be the hadronically decaying tau (or tau-like jet).We split the $\gamma + jet$ sample into subsamples for several $E^c l_T$ intervals and repeat the procedure described above, applying the $E^c l_T$-dependent rescaling to the MC. The observed difference is rather small.

Based on this study we assign a systematic uncertainty of 1 % due to the effect of $\not\!\!E_T$ on the event selection cuts.

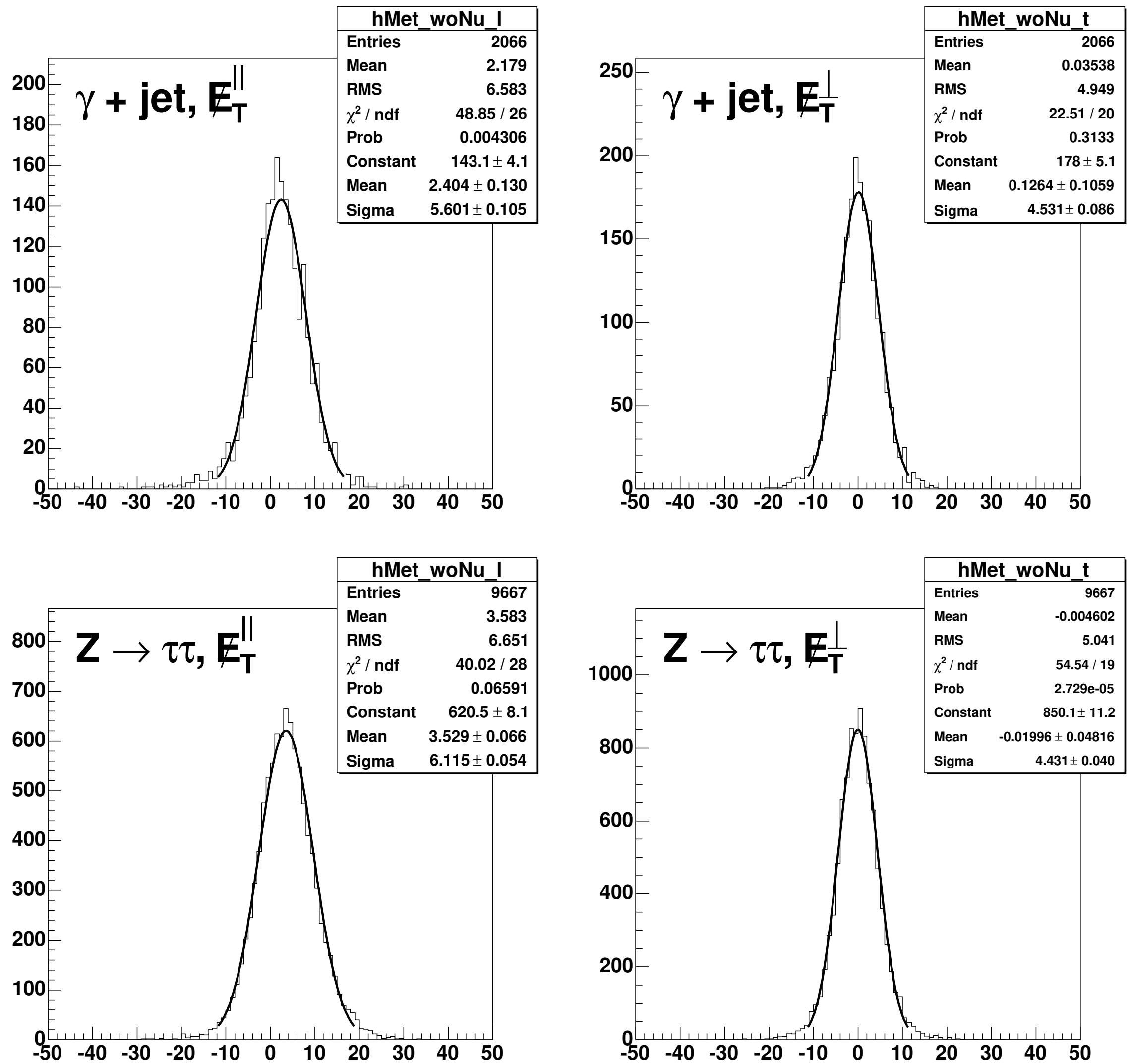

Figure 27: *Parallel and transverse components of* $\not\!\!E_T$ *with respect to tau (tau-like jet) for* $Z \to \tau_e\tau_h$ *MC and* $\gamma + jet$ *as indicated on the plots.* $\not\!\!E_T$ *in MC was corrected for the contribution from the neutrinos.*

F Tau Energy Scaling and Uncertainty

The determination of the tau energy scale is a challenging undertaking. Due to the the accompanying neutrinos one has to rely on indirect methods, like $\gamma + jet$ balancing using tau-like jets to approximate real taus. These methods can be used to set teh absolute scale. In many cases, however, the absolute energy scale (although desirable) is not absolutely needed. What is important is to have the data/MC agree on the prediction of the reconstructed E(trks $+ \pi^0$'s). If we do not attempt to extract absolute measurements of quantities such as Z or Higgs mass, absolute energy scales (and the associated uncertainties) do have large impact. What really matters is th relative data/MC energy scale. This simplifies the problem, but does not eliminate all hurdles. The neutrinos still prevent us making comparisons of distributions produced on tau-by-tau bases. Backgrounds and statistics are not on our side either.

Here we use a comparison of the data and MC p_T distributions of reconstructed taus in $W \to \tau\nu$ decays. The data sample, selection and bg estimation are as in Appendix C. Figure 28 shows the P_T distribution for data, signal MC and backgrounds. QCD backgrounds ($jet \to \tau$ fakes are not included. There are two limiting cases: assume the small shape difference is due to not including QCD on the plot, or that it is entirely due to some data/MC difference. This limiting cases give as a measure of the data/MC agreement. Figure 29 shows a comparison of the p_T spectrum after applying 0.98 scale factor to MC.

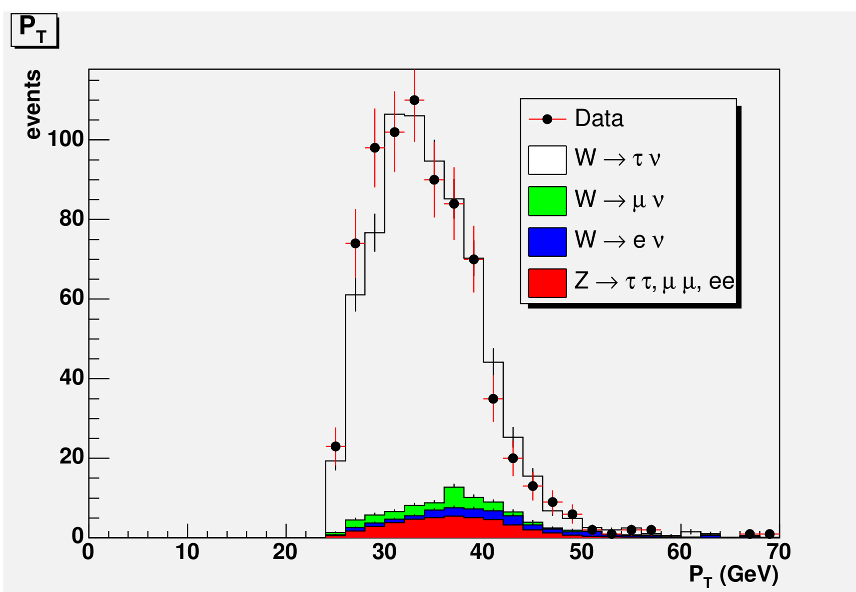

Figure 28: *p_T spectrum of taus from W decays.*

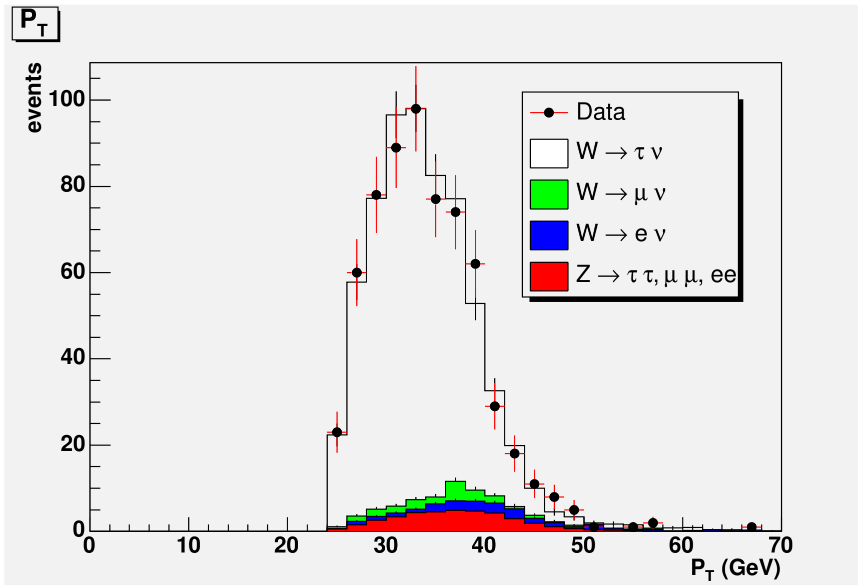

Figure 29: *p_T spectrum of taus from W decays. The MC energy has been scaled by 0.98.*

We compare the p_T shapes of the MC and background-subtracted data after normalization using a χ^2 test:

$$\chi^2 = \sum_i \frac{(n_i^{data} - n_i^{MC})^2}{\sigma^2_{n_i^{data}} + \sigma^2_{n_i^{MC}}},$$

where the sum goes over the bins of the $p_T$distribution. We perform the test for scaling factors for reconstructed MC trks+π^0's energy ranging from 0.9 to 1.1.

Figure 30 shows the χ^2 as a function of the scaling factor. Under the "no QCD", hypothesis the minimum is reached at scaling factor 0.982. We take a 2% data/MC energy scale uncertainty and use this value to study the effects on the projected Higgs production limits [11].

The rescaling procedure described above does not attempt to identify the source of the shift (assuming it is real, and not resulting from a fluctuation or QCD contribution). The tau energy as used in this note is determined by tracks and reconstructed π^0's. The agreement between data and MC in track momentum measurement is expected to be very good. Reconstructed π^0's use CEM calorimeter energy which is also well simulated. What is really challenging to determine, is looses due to different efficiency of π^0 reconstruction in data and

[11]The error assignment is probably on the conservative side. We expect that taking into account QCD contributions will produce a better estimate of the data/MC tau energy scaling factor. Since the QCD appears in the lower end of the p_T spectrum, the scaling factor will move closer to 1.0.

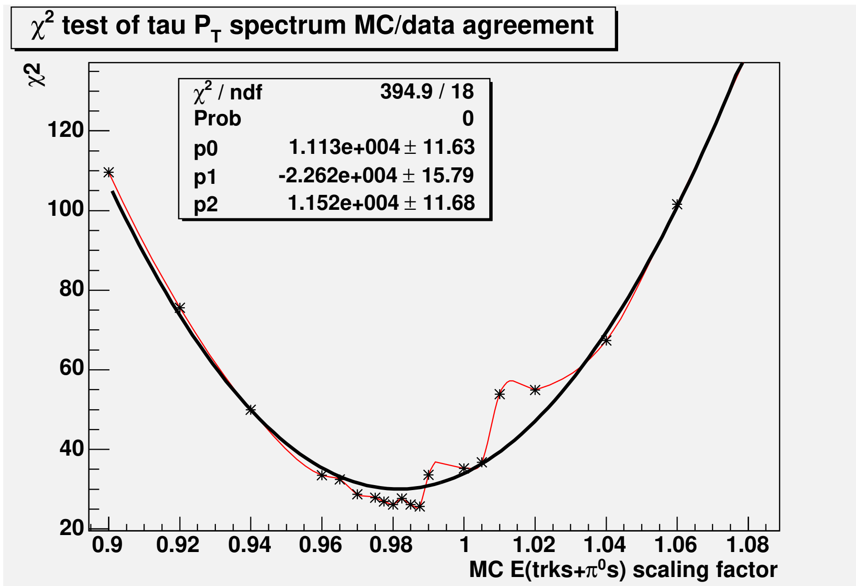

Figure 30: χ^2 *as a function of tau energy scaling factor applied to MC.*

MC. There are known deficiencies in CES simulation that may have some impact. Some of them are discussed in [8] and need to be addressed. It is also important to stress that these differences do not directly lead to energy underestimation in data. Another argument for possible larger π^0 losses in data is presence of dead CES strips/wires that are not simulated.

We study the impact of possible larger losses of π^0's in data by random elimination of reconstructed $\pi 0$'s in MC. Random removal $\pi 0$'s is an exaggerated simulation of the losses. In this scheme, every removal of a π^0 results in energy loss. In reality, a loss of a π^0 in a tower containing another one, results in its energy being assigned to its neighbor, not in a loss. Nevertheless, this procedure will give us an idea of the impact of losses on the estimated limits.

We have simulated π^0 losses with probability 5, 10, 15%, and examined the impact on the limits compared to the overall 2% tau energy shift. In all cases we observed smaller effect.

Because of the preliminary nature of the presented results, we decided on a conservative approach and chose to use the 2% tau energy shift for our systematics.